

Frustrated spin chains in strong magnetic field: dilute two-component Bose gas regime

A. K. Kolezhuk,^{1,2} F. Heidrich-Meisner,³ S. Greschner,⁴ and T. Vekua⁴

¹*Institute of Magnetism, National Academy of Sciences and Ministry of Education, 36-b Vernadskii av., 03142 Kiev, Ukraine*

²*Institute of High Technologies, T. Shevchenko Kiev National University, 64 Volodymyrska str., 01601 Kiev, Ukraine*

³*Department of Physics and Arnold Sommerfeld Center for Theoretical Physics,
Ludwig-Maximilians-Universität München, D-80333 München, Germany*

⁴*Institut für Theoretische Physik, Leibniz Universität Hannover, Appelstr. 2, 30167 Hannover, Germany*

(Dated: April 4, 2012)

We study the ground state of frustrated spin- S chains in a strong magnetic field in the immediate vicinity of saturation. In strongly frustrated chains, the magnon dispersion has two degenerate minima at inequivalent momenta $\pm Q$, and just below the saturation field the system can be effectively represented as a dilute one-dimensional lattice gas of two species of bosons that correspond to magnons with momenta around $\pm Q$. We present a theory of effective interactions in such a dilute magnon gas that allows us to make quantitative predictions for arbitrary values of the spin. With the help of this method, we are able to establish the magnetic phase diagram of frustrated chains close to saturation and study phase transitions between several nontrivial states, including a two-component Luttinger liquid, a vector chiral phase, and phases with bound magnons. We study those phase transitions numerically and find a good agreement with our analytical predictions.

PACS numbers: 75.10.Jm, 75.30.Kz, 75.40.Mg, 67.85.Hj

I. INTRODUCTION

Frustrated spin systems have been an object of avid interest to researchers for several decades. In low dimensions, the interplay of frustration and quantum fluctuations proved to be favorable for generating states with unconventional spin order, such as chiral, nematic, or general multipolar phases, as well as for the existence of various disordered states. A strong external magnetic field competes with the exchange interaction, inducing a rich variety of phase transitions. An overview of this rapidly progressing field may be found in Refs. 1 and 2.

A spin chain with competing nearest and next-nearest neighbor exchange interaction represents a paradigmatic model of frustrated spin systems in one dimension. Despite many years of extensive studies, it continues to deliver fresh surprises. The frustrated spin- S chain model, which will be the main subject of our study, is described by the following Hamiltonian:

$$\mathcal{H} = \sum_n \left\{ \frac{J_1}{2} (S_n^+ S_{n+1}^- + S_n^- S_{n+1}^+) + J_1^z S_n^z S_{n+1}^z - H S_n^z \right. \\ \left. + \frac{J_2}{2} (S_n^+ S_{n+2}^- + S_n^- S_{n+2}^+) + J_2^z S_n^z S_{n+2}^z \right\}, \quad (1)$$

where (S_n^\pm, S_n^z) are spin- S operators acting at site n of a one-dimensional lattice, J_1, J_1^z and J_2, J_2^z are nearest-neighbor (NN) and next-nearest neighbor (NNN) exchange interactions, and H is the external magnetic field. In this paper, we are interested in the frustrated case, so J_2 is chosen to be positive and the sign of J_1 is arbitrary. It is convenient to use the quantity

$$\beta = J_1/J_2 \quad (2)$$

as the frustration parameter. The system may be alternatively viewed as two antiferromagnetic chains connected by ferro- or antiferromagnetic zigzag couplings J_1, J_1^z .

For $S = \frac{1}{2}$, the above model has been extensively studied. Its isotropic ($J_1^z = J_1, J_2^z = J_2$) version has a rich magnetic phase diagram exhibiting states with competing unconventional orders, both for a ferromagnetic³⁻⁷ and an antiferromagnetic⁸⁻¹² NN exchange interaction J_1 . In particular, the vector chirality (VC), which is a quantum remnant of the classical helical spin order and is equivalent to the local spin current, competes, on the one hand, with multipolar orders characterizing quasi-condensates consisting of multimagnon bound states, and, on the other hand, with the two-component Tomonaga-Luttinger liquid (TLL2)¹³ where the two components correspond to magnons with momenta around two degenerate dispersion minima at inequivalent points in the Brillouin zone. The same set of phases has been found in the anisotropic version of the model as well.¹⁴

The model (1) with $S = \frac{1}{2}$ and a ferromagnetic (FM) NN coupling has been discussed recently in connection with the description of several quasi one-dimensional magnetic materials such as LiCuVO₄ (Ref. 15–18), Rb₂Cu₂Mo₃O₁₂ (Ref. 19), Li₂ZrCuO₄ (Ref. 20), and anhydrous CuCl₂ (Ref. 21).

For higher values of S , not much is known about the magnetic phase diagram of frustrated chains. A theoretical approach based on bosonization⁹ predicts that in the regime of two weakly coupled antiferromagnetic (AF) chains ($|\beta| \ll 1$) a VC phase completely fills the magnetic phase diagram for all nonvanishing values of the magnetization between zero and saturation. On the FM side ($\beta < 0$), for spin- $S \geq 1$ chains right below the saturation field, a recent large- S analysis in the framework of a dilute magnon gas approach²² predicts the existence of either a VC phase, for $\beta_{cr}(S) < \beta < 0$, or a metamagnetic magnetization jump, for $-4 < \beta < \beta_{cr}(S)$, with $\beta_{cr}(S \geq 6) = -4$. Numerical studies of magnetization curves²³ have established the universal presence of a mag-

netization plateau at one third of the saturation value in antiferromagnetic chains with $S = 1, \frac{3}{2},$ and 2 , while a metamagnetic jump at saturation has been found in FM chains²² for $S = 1$ and $S = \frac{3}{2}$ (metamagnetic jumps have been observed earlier in $S = \frac{1}{2}$ chains⁷ as well, particularly at saturation for $\beta \rightarrow -4$). The numerical analysis of correlation functions^{10,24} has been limited to cuts at the fixed value of the frustration parameter $\beta = 1$, and has led to the conclusion that the field-induced VC phase is present in AF chains with higher S as well (values up to $S = 2$ have been studied). The TLL2 phase has been observed in $S = \frac{1}{2}$ frustrated AF chains^{8,11–13}, in anisotropic $S = \frac{1}{2}$ frustrated FM chain,¹⁴ as well as in $S = 1$ chain with bilinear and biquadratic exchange.^{13,25} Indications of its existence have also been found in the form of kinks in magnetization curves in higher- S frustrated AF chains.²³

In this paper, we study the ground state of a strongly frustrated ($|\beta| < 4$) spin- S chain (1) in strong magnetic fields in the immediate vicinity of saturation. Just below the saturation field, the system can be represented as a dilute lattice gas of magnons, and since in the case of strong frustration the magnon dispersion has two degenerate minima at inequivalent points $\pm Q$ in momentum space, this lattice gas is effectively a two-component one. We present a theory of effective interactions in such a dilute magnon gas that is especially adapted to the one-dimensional case, does not involve an $1/S$ expansion, and thus allows us to draw quantitative predictions for arbitrary spin. We establish the magnetic phase diagram of isotropic and anisotropic frustrated chains close to saturation and study phase transitions between several non-trivial states, including TLL2 and VC phases, and phases with bound magnons. Particularly, we show that the TLL2 phase appears in FM and AF chains for all values of the spin S . We complement our analytical results with density matrix renormalization group^{26,27} (DMRG) simulations. Specifically, we compute the central charge as a function of β (at fixed magnetization close to the saturation value), which allows us to locate phase transitions between one- and two-component states. In order to identify those one-component states that have vector chiral order, we further calculate the chirality. Our DMRG results for the transition from the VC to the TLL2 phase are in a good agreement with our theoretical predictions.

The structure of the paper is as follows: in Sect. II we describe mapping of the spin problem to the dilute two-component lattice Bose gas and present the theory allowing us to calculate effective interactions in such a gas for general spin S . In Sect. III, the two-magnon scattering problem in a frustrated chain is considered, and its links to the effective theory of Sect. II are established. Section IV discusses the specific predictions of the theory for frustrated spin chain models with different S and either isotropic or anisotropic exchange interactions, while Sect. V presents the results of numerical analysis and their comparison with analytical predictions. Finally, Sect. VI contains a brief summary.

II. EFFECTIVE TWO-COMPONENT BOSE GAS MODEL

We are interested in the interactions between magnons in the regime of a dilute magnon gas, i.e., for values of the field H just slightly below the saturation field H_s . Because of the diluteness of the gas, two-body interactions dominate. It is convenient to use the Dyson-Maleev representation²⁸ for the spin operators in (1):

$$\begin{aligned} S_n^+ &= \sqrt{2S}b_n, & S_n^- &= \sqrt{2S}b_n^\dagger \left(1 - \frac{b_n^\dagger b_n}{2S}\right), \\ S_n^z &= S - b_n^\dagger b_n, \end{aligned} \quad (3)$$

where b_n are bosonic operators acting at site n . To enforce the constraint $b_n^\dagger b_n \leq 2S$, one can add the infinite interaction term to the Hamiltonian, which reads:

$$\mathcal{H} \mapsto \mathcal{H} + U \sum_n : (b_n^\dagger b_n)^{2S+1} : , \quad U \rightarrow +\infty, \quad (4)$$

where $: (\dots) :$ denotes normal ordering. Obviously, at the level of two-body interactions this term is important only for $S = \frac{1}{2}$.

Passing further to the momentum representation for bosonic operators, one can rewrite the model (1) in the following form:

$$\mathcal{H} = \sum_k (\varepsilon_k - \mu) b_k^\dagger b_k + \frac{1}{2L} \sum_{kk'q} V_q(k, k') b_{k+q}^\dagger b_{k'-q}^\dagger b_k b_{k'}. \quad (5)$$

Here L is the total number of lattice sites, the chemical potential is $\mu = H_s - H$, where

$$H_s = 2SJ_2(1 + \beta^2/8) + 2S(J_1^z + J_2^z)$$

is the saturation field²⁹ for the case of a strong NNN interaction $|J_1| \leq 4J_2$, which is of our main interest here. The magnon energy

$$\varepsilon_k = 2S(J_1 \cos k + J_2 \cos 2k - J_1^z - J_2^z) + H_s \quad (6)$$

is defined in a way that ensures that $\min \varepsilon_k = 0$. The lattice constant has been set to unity. It is easy to convince oneself that ε_k does not depend on $J_{1,2}^z$. The dispersion ε_k has two degenerate minima at $k = \pm Q$, where

$$Q = \arccos[-\beta/4].$$

The two-body interaction $V_q(k, k')$ generally depends on the transferred momentum q as well as on the incoming momenta k, k' :

$$V_q(k, k') = \begin{cases} J^z(q) - \frac{1}{2}[J(k) + J(k')] & S \geq 1, \\ U + J^z(q), & U \rightarrow +\infty \quad S = \frac{1}{2} \end{cases}, \quad (7)$$

where

$$\begin{aligned} J(k) &= 2J_1 \cos k + 2J_2 \cos 2k, \\ J^z(k) &= 2J_1^z \cos k + 2J_2^z \cos 2k. \end{aligned} \quad (8)$$

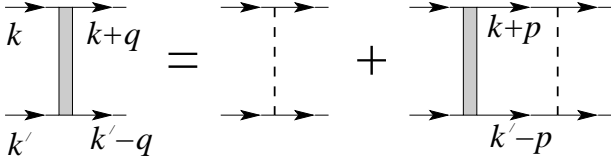


FIG. 1. The ladder approximation to the Bethe-Salpeter equation for the renormalized two-body interaction vertex $\Gamma_q(k, k'; E)$. Solid lines denote bare propagators. The approximation becomes exact at $\mu \rightarrow 0$.

It is easy to see that in this notation $\varepsilon_k = S[J(k) - J(Q)]$.

The model (5) defines a gas of bosons with a nontrivial double-minima dispersion, on a one-dimensional (1d) lattice. We are interested in the renormalized two-body interaction in this gas in the dilute limit, i.e., $\mu \rightarrow 0$. In the $\mu \rightarrow 0$ limit, the self-energy vanishes,³⁰ so the full propagator coincides with the bare one. Then, the Bethe-Salpeter (BS) equation for the renormalized two-body interaction vertex $\Gamma_q(k, k'; E)$ (where E is the total energy of the incoming particles) in the limit $\mu \rightarrow 0$ takes the following simple form:³¹

$$\Gamma_q(k, k'; E) = V_q(k, k') - \frac{1}{L} \sum_p \frac{V_{q-p}(k+p, k'-p) \Gamma_p(k, k'; E)}{\varepsilon_{k+p} + \varepsilon_{k'-p} - E}. \quad (9)$$

This expression is schematically shown in terms of Feynman diagrams in Fig. (1). For the physical “on-shell” vertex the energy is fixed at $E = \varepsilon_k + \varepsilon_{k'}$, but we keep Eq. (9) in a general form for reasons that will become clear shortly.

At a low density of magnons (small chemical potential μ) the system is mainly populated by particles with momenta around the two dispersion minima at $\pm Q$, which at low energies can be interpreted as two different bosonic flavors. One can obtain the low-energy effective theory in the form of the Gross-Pitaevsky-type energy functional for two-component field (for the outline of the derivation, see Appendix A):

$$\mathcal{H}_{\text{GP}} = \int dx \left\{ \sum_{a=1,2} \frac{|\nabla \Phi^a|^2}{2m} + \frac{1}{2} \Gamma_{11}^\Lambda (n_1^2 + n_2^2) + \Gamma_{12}^\Lambda n_1 n_2 - \mu(n_1 + n_2) \right\}. \quad (10)$$

Here $\Phi^{1,2}$ are the macroscopic bosonic fields that describe magnons with momenta k lying within the intervals $|k \pm Q| < \Lambda$ around the dispersion minima, Λ is an infrared cutoff, and $n_a = |\Phi^a|^2$ are the corresponding densities. Both bosonic species have the same effective mass

$$m = \left(\frac{\partial^2 \varepsilon_k}{\partial k^2} \Big|_{k=Q} \right)^{-1} = \frac{2}{SJ_2(16 - \beta^2)}. \quad (11)$$

For the sake of clarity, the Planck constant is set to unity.

The macroscopic couplings Γ_{ab}^Λ are given by

$$\begin{aligned} \Gamma_{11}^\Lambda &= \Gamma_0^\Lambda(Q, Q; 0), \\ \Gamma_{12}^\Lambda &= \Gamma_0^\Lambda(-Q, Q; 0) + \Gamma_{2Q}^\Lambda(-Q, Q; 0) \end{aligned} \quad (12)$$

where the vertex function $\Gamma_q(k, k'; E)$ is the solution of the BS equation (9) with the infrared cutoff $|p| > \Lambda$ introduced into the sum over transferred momentum p .

As noticed first by Batyev and Braginskii,³¹ for a model with short-range interaction the solution of (9) can be expressed in terms of a finite number of Fourier harmonics in the transferred momentum. In our case, from the structure of $V_q(k, k')$ it is easy to see that $\Gamma_q(k, k'; E)$ generally contains harmonics proportional to 1, $\cos q$, $\sin q$, $\cos 2q$, and $\sin 2q$. The integral equation thus is reduced to a system of five linear equations that can be solved for general spin S , thus no $1/S$ expansion is necessary. For the purpose of finding only the effective couplings Γ_{11} , Γ_{12} , the number of linear equations in the general problem outlined above can be reduced from five to three, see Appendix B.

The point $\Gamma_{11} = \Gamma_{12}$ corresponds to the enhanced $SU(2)$ symmetry at the level of the effective low-energy theory. For $\Gamma_{12} < \Gamma_{11}$, the ground state of the gas contains an equal density of the two particle species, and for $\Gamma_{12} > \Gamma_{11}$ just one of the two species is present in the ground state. Recall that in our spin problem the total number of each species is not separately fixed, in contrast to a typical setup for atomic Bose mixtures. In a setup with fixed particle numbers the ground state at $\Gamma_{12} < \Gamma_{11}$ is in the mixed phase, and $\Gamma_{12} > \Gamma_{11}$ corresponds to phase separation. In the spin language, in two or three dimensions the state with only one bosonic species corresponds to the helical magnetic order, while the state with an equal density of the two species corresponds to the “fan” phase with coplanar spin order.³² In one dimension, no long-range order is possible, and the state with only one species can be identified with the vector chiral (VC) phase,⁹ while the two-species state corresponds to the two-component Tomonaga-Luttinger (TLL2) liquid.^{13,25}

The approach that we have just described is well-known in the physics of magnetism in a strong field^{31–37} and is rather straightforward for three-dimensional systems where in the limit $\Lambda \rightarrow 0$ the couplings Γ_{ab}^Λ are well defined and acquire finite values. In the case of low dimensions, however, for $\Lambda \rightarrow 0$ the integral in Eq. (9) diverges at $p = 0$ for $(k, k') = (Q, Q)$, and for $(k, k') = (-Q, Q)$ there are divergences both at $p = 0$ and $p = 2Q$. Thus, the above scheme needs a modification in the low-dimensional case. The couplings Γ_{ab}^Λ can be interpreted as functions of the running cutoff Λ in the spirit of the renormalization group (RG) approach. The RG flow is then interrupted at a certain scale $\Lambda = \Lambda_*$ that depends on the particle density. This approach has proved to be quite successful for one-component Bose gas.^{38–41} The focus of our study here is to extend this approach to the two-component gas, which, as we have

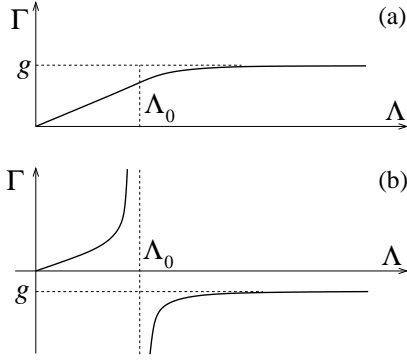


FIG. 2. The typical behavior of the running coupling constant Γ as a function of the infrared cutoff Λ , in a *continuum* model of a Bose gas with a bare contact interaction g (i.e., the two-body interaction potential is approximated by the delta-function $U(x) = g\delta(x)$): (a) for the case of the repulsive coupling $g > 0$, (b) for the case of attraction $g < 0$.

seen, is of special interest for frustrated systems. In this paper, we concentrate on the one-dimensional case.

Solving the BS equation (9), one can show that the expansion of Γ_{ab}^Λ as a series in Λ has the following form:

$$\begin{aligned}\frac{1}{\Gamma_{11}^\Lambda} &= \frac{m}{\pi\Lambda} + \frac{1}{g_{11}} + O(\Lambda) + \dots, \\ \frac{1}{\Gamma_{12}^\Lambda} &= \frac{m}{\pi\Lambda} + \frac{1}{g_{12}} + O(\Lambda) + \dots\end{aligned}\quad (13)$$

Note that the expansion starts with the term proportional to $1/\Lambda$ that turns out to be the same for both couplings. Thus, for $\Lambda \rightarrow 0$ both $\Gamma_{11}^\Lambda/\Lambda$ and $\Gamma_{12}^\Lambda/\Lambda$ flow to the same universal value, which reflects the tendency of the RG flow to restore the $SU(2)$ symmetry for the two-component Bose mixture.⁴²

The parameters g_{11} , g_{12} , which determine the second term in the expansions (13), have a special meaning: under certain conditions they can be identified (see Appendices A,C) with the effective bare coupling constants of the *continuum* two-component Bose gas with a contact interaction $g_{11}\delta(x-x')$ between the same species (here $\delta(x)$ is the Dirac delta-function) and an interaction of the form $g_{12}\delta(x-x')$ between different species. Such a continuum model is essentially the two-component Lieb-Liniger model. The behavior of running couplings Γ_{ab}^Λ in this problem is exactly given by the first two terms in Eq. (13).⁴² In the semiclassical limit $S \rightarrow \infty$, the parameters g_{ab} are given by simple expressions⁴³

$$\begin{aligned}g_{11} &= \beta^2/4 + 2(1 + J_2^z + J_1^z) = H_s/S, \\ g_{12} &= \frac{J_2^z \beta^4}{16} + \beta^2\left(\frac{1}{2} + \frac{J_1^z}{4} - J_2^z\right) + 4(J_2^z + 1).\end{aligned}\quad (14)$$

Typical behavior of Γ_{ab}^Λ for the Lieb-Liniger model is shown in Fig. 2. It is clear that Γ_{ab} changes its behavior on the characteristic scale $\Lambda_0 \sim g_{ab}m$. For the repulsive case ($g_{ab} > 0$) this is simply the scale at which the renormalized coupling Γ_{ab}^Λ starts to deviate considerably from

its bare value, while for the case of attraction ($g_{ab} < 0$) the renormalized coupling has a pole at $\Lambda = \Lambda_0$ that technically limits the RG flow and physically indicates the existence of bound states with energy $E_b \sim \Lambda_0^2/2m$.

It is important to realize the following: since we actually deal with a *lattice* problem that has a natural ultraviolet cutoff $\Lambda_{UV} \sim 1$, the interpretation of g_{ab} as physical bare couplings makes sense only if the condition

$$|g_{11}|m \ll 1, \quad |g_{12}|m \ll 1 \quad (15)$$

is satisfied (see Appendix C for more details). If the above condition of weak coupling is broken, parameters g_{ab} cannot be interpreted as physical bare couplings, and only the fully renormalized interactions

$$\Gamma_{ab} = \Gamma_{ab}^{\Lambda=\Lambda_*}$$

retain their meaning as effective low-energy coupling constants. For instance, if $g_{ab} < 0$ but $|g_{ab}|m \gtrsim 1$, there is no attraction in the lattice problem and no bound states are present: directly looking at the behavior of Γ_{ab}^Λ for the lattice problem, one can convince oneself that there is no pole in Λ . In the strong coupling regime $|g_{ab}|m \gtrsim 1$ the sign of g_{ab} merely determines the curvature of the Γ_{ab}^Λ dependence near $\Lambda = 0$, but the renormalized coupling itself remains positive. The only physical meaning of g_{ab} in such a case is that they are connected to the asymptotic phase shift of scattering states at small transferred momenta, see Sect. III below.

The scale Λ_* , at which the RG flow has to be interrupted, can be easily fixed from the well-known exact result for the single-component dilute Bose gas:⁴⁴ in the limit $\mu \rightarrow 0$ the particle density n must behave as

$$n = (2m\mu/\pi^2)^{1/2}. \quad (16)$$

Indeed, in the phase with only one bosonic species, which corresponds to $\Gamma_{12} > \Gamma_{11}$, the density of particles obtained from the semiclassical description of Eq. (10) is $n = \mu/\Gamma_{11}$, so in order to fulfill Eq. (16), one has to assume that at $\mu \rightarrow 0$ the effective coupling behaves as $\Gamma_{11} \rightarrow \pi\sqrt{\mu/(2m)}$ and thus

$$\Lambda_* = \sqrt{\mu m/2}. \quad (17)$$

In the phase with equal densities of different species, which corresponds to $\Gamma_{12} < \Gamma_{11}$, the total density at the semiclassical level of Eq. (10) is $n = 2\mu/(\Gamma_{11} + \Gamma_{12})$. It follows from Eq. (13) that for $\mu \rightarrow 0$ the behavior of the density is described by the same expression (16) as for the one-component gas. Thus, at the transition from the vector chiral phase to the two-component TL liquid, in the regime of a low magnon density there is no magnetization kink (cusp), in agreement with numerical results.^{8,11,14} The reason for that is the effective fermionization of the magnon gas and formation of a single Fermi sea at low densities, see the discussion below in Sect. III.

From Eqs. (13) one can see that the transition point between the TLL2 and VC phases, that is determined by

the condition $\Gamma_{11} = \Gamma_{12}$, can be detected by the *crossing* of g_{12} and g_{11} (i.e., a change of sign of $g_{12} - g_{11}$ that may happen if one of the couplings goes through a pole does not correspond to a phase transition). We will consider specific examples below in Sect. IV.

There is another way of calculating the renormalized interaction in low dimensions, which avoids introducing the infrared cutoff. In Refs. 45 and 46 it has been shown that a good approximation to the correct “many-body” expression for the effective four-point vertex function (i.e., the two-particle scattering amplitude in the presence of a finite particle density) at low energy $\Gamma_q^{MB}(k, k'; E \rightarrow 0)$ can be obtained from the “bare” two-particle scattering amplitude $\Gamma_q(k, k'; E)$ taken at a finite *negative* energy $E = -E_*$ that is proportional to the chemical potential μ :

$$\Gamma_q^{MB}(k, k'; E \rightarrow 0) \approx \Gamma_q(k, k'; -E_*), \quad E_* = C\mu. \quad (18)$$

Here the coefficient C turns out to depend on the dimension d of the problem: for $d = 2$ one obtains $C = 1$, and $C = \pi^2/8$ for $d = 1$. The two-particle scattering amplitude $\Gamma_q(k, k'; E)$ is precisely the solution of Eq. (9) since $\mu = 0$ means that no other particles are present except for the two that scatter off each other.

Following this scheme, we can define the energy-dependent coupling constants as

$$\begin{aligned} \Gamma_{11}(E) &= \Gamma_0(Q, Q; E), \\ \Gamma_{12}(E) &= \Gamma_0(-Q, Q; E) + \Gamma_{2Q}(-Q, Q; E) \end{aligned} \quad (19)$$

(note that the expressions on the rhs of Eq. (19) are now calculated without any infrared cutoff). Solving the BS equation in the symmetrized form (B2), (B3) for $\Gamma_{ab}(-E_*)$, one can show that the expansion of $\Gamma_{ab}^{-1}(-E_*)$ in E_* has the following structure:

$$\begin{aligned} \frac{1}{\Gamma_{11}(-E_*)} &= \left(\frac{m}{4E_*} \right)^{1/2} + \frac{1}{g_{11}} + O(E_*^{1/2}) + \dots, \\ \frac{1}{\Gamma_{12}(-E_*)} &= \left(\frac{m}{4E_*} \right)^{1/2} + \frac{1}{g_{12}} + O(E_*^{1/2}) + \dots \end{aligned} \quad (20)$$

The similarity with the expansion in the infrared cutoff, i.e., Eq. (13), is obvious. Replacing E_* with its 1d value $E_* = \pi^2\mu/8$, one can readily convince oneself that

$$\Gamma_{ab}^{\Lambda_*} = \Gamma_{ab}(-E_*) + O(\mu^{3/2}), \quad (21)$$

i.e., both regularization methods yield equivalent results in the dilute limit $\mu \rightarrow 0$. However, for practical purposes, the off-shell method is more convenient since it allows an easier calculation of all integrals involved.

III. TWO-MAGNON PROBLEM IN FRUSTRATED SPIN CHAINS

A general two-magnon state with the total quasi-momentum K can be written in the form

$$|\Psi_K\rangle = \sum_{n,r \geq 0} C_r e^{iK(n+\frac{r}{2})} \frac{S_n^- S_{n+r}^- |F\rangle}{\langle F | S_{n+r}^+ S_n^+ S_n^- S_{n+r}^- | F \rangle},$$

where $|F\rangle$ is the fully polarized state. The Schrödinger equation for the two-magnon problem leads to a coupled system of equations for the amplitudes C_r , presented in Appendix D, that is a generalization of the one for the case of an $SU(2)$ symmetric exchange.²² Both scattering states and bound states of two magnons can be obtained from the solution of this system. The bound states can be obtained along the lines derived for an $SU(2)$ symmetric exchange.²² Here we discuss the solutions for the case of continuum states that describe scattering of two magnons with momenta k_1, k_2 .

Solving this scattering problem, we have to distinguish two cases. In the first case the problem is non-degenerate, meaning that for a given total momentum $K = k_1 + k_2$ and energy E there is only one scattering state. This will be realized when the momenta of the two magnons participating in the scattering are in the vicinity of the same dispersion minimum, e.g., $k_1 = Q + k$, and $k_2 = Q - k$. In this non-degenerate case the system (D3) can be solved by using the following ansatz:

$$C_r = \cos(kr + \delta_{11}) + ve^{-\kappa_0 r}, \quad r \geq 1. \quad (22)$$

This ansatz satisfies the recurrence relation in Eqs. (D3), for ($r \geq 3$) if κ_0 is a root of the following equation:

$$J_1 \cos \frac{K}{2} (\cos k - \cosh \kappa_0) + J_2 \cos K (\cos 2k - \cosh 2\kappa_0) = 0. \quad (23)$$

Furthermore, to be a physically acceptable solution, the correct root should satisfy $\text{Re}[\kappa_0] > 0$. The three unknown constants C_0 , v , and δ_{11} are determined from the first three equations of (D3).

To extract the scattering length a_{11} from the phase shift δ_{11} , one can use the same relation as found in the one-dimensional continuum model of a one-component Bose gas interacting via a short-range potential, namely $\delta_{11}(k) \rightarrow -\frac{\pi}{2} - a_{11}k$ at $k \rightarrow 0$, or, in a different form,

$$a_{11} = \lim_{k \rightarrow 0} [\cot(\delta_{11})/k]. \quad (24)$$

If the short-range potential between two particles of mass m with coordinates x, x' is approximated by the contact potential of the form $U(x - x') = g_{11}\delta(x - x')$, then the scattering length a_{11} is connected to the bare coupling g_{11} as follows:⁴⁷

$$g_{11} = -2/(a_{11}m). \quad (25)$$

In the second case, there is more than one scattering state for a given energy and total momentum. This degeneracy stems from the parity symmetry and the double-minimum structure of the single-magnon dispersion. This case will be realized if the momenta of two scattering magnons are in the vicinity of two different dispersion minima. For instance, the state with the total momentum $K = 0$ that corresponds to $k_1 = Q + p$, $k_2 = -Q - p$ (half relative momentum $k = Q + p$) is degenerate with another scattering state with $k_1 = Q - \tilde{p}$,

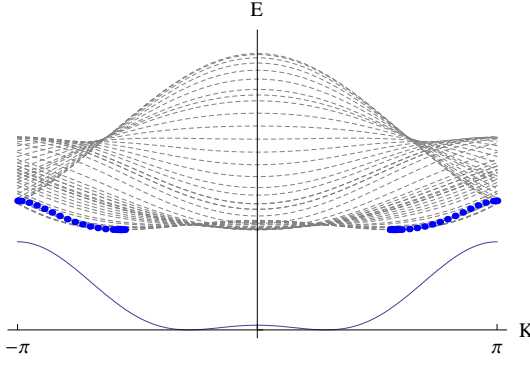


FIG. 3. (Color online). Single magnon and two-magnon spectra for the isotropic spin-1 chain with $\beta = -2.5$ at the field $H > H_s$, as a function of the total momentum K . The solid line shows the single-magnon dispersion with minima at $\pm Q$. One can clearly see degeneracies of the scattering states in the vicinity of the lower bound of the two-particle continuum for $K = 0$ as well as in some high-energy regions. A peculiar feature of the spectrum is the existence of a stable two-magnon bound state inside the continuum of scattering states (this happens for any spin $S > \frac{1}{2}$ and $\beta < 0$). The procedure of finding two-magnon bound states in isotropic ferromagnetic $S > \frac{1}{2}$ frustrated chains was discussed in detail in Ref. 22, and here we include them for the sake of completeness.

$k_2 = -Q + \tilde{p}$ (half relative momentum $\tilde{k} = Q - \tilde{p}$). This degeneracy is visible at the lower bound of the two-magnon scattering continuum around $K \simeq 0$, depicted in Fig. 3. Generally, $\tilde{p} \neq p$ because the shape of the one-magnon dispersion curve is not exactly symmetric around the minima at $\pm Q$, but $\tilde{p} \rightarrow p$ at $p \rightarrow 0$. The relative momenta k, \tilde{k} of two degenerate states with the same total momentum K are connected by the equation

$$J_1 \cos \frac{K}{2} (\cos k - \cos \tilde{k}) + J_2 \cos K (\cos 2k - \cos 2\tilde{k}) = 0. \quad (26)$$

For $K = 0$ the solution of the above equation takes the form

$$\tilde{k} = \arccos(2 \cos Q - \cos k), \quad (27)$$

from which, in particular, it follows that for $p \equiv (k - Q) \rightarrow 0$ one has $\tilde{p} \equiv (Q - \tilde{k}) = p + O(p^2)$.

The Schrödinger equation for the scattering states Eq. (D3) is in this case solved by the following ansatz:

$$C_r = \cos(kr + \alpha(k)) + v(k) \sin(\tilde{k}r), \quad r \geq 1. \quad (28)$$

From the form of the scattering state Eq. (28) it follows that if one prepares the incoming state of two magnons at $t \rightarrow -\infty$ with relative momentum k , the outgoing state at $t \rightarrow +\infty$ will be a superposition of states with relative momenta k and \tilde{k} .

To determine the three unknown quantities C_0, α , and v we again use the first three equations of Eq. (D3). In

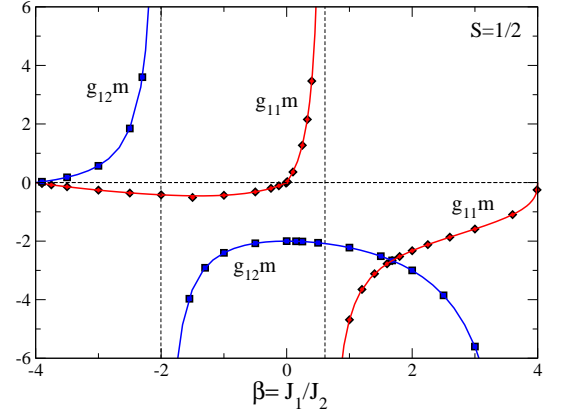


FIG. 4. (Color online). Bare coupling constants for $S = 1/2$: solid lines correspond to the calculation based on the regularized Bethe-Salpeter equation, while symbols show the results extracted from the solution of two-magnon scattering problem. In the region $\beta > 0.614$, the intraspecies coupling g_{11} enters the super-Tonks regime. The interspecies coupling g_{12} enters the super-Tonks regime in the region $\beta > -2$.

Appendix E we show how to extract the interspecies scattering phase shift

$$\delta_{12} = -\arccos \frac{\cos \alpha}{\sqrt{\cos^2 \alpha + (v + \sin \alpha)^2}} \quad (29)$$

from the scattering state Eq. (28). The scattering length is then obtained in analogy to the case of the intraspecies scattering,

$$a_{12} = \lim_{p \rightarrow 0} [\cot(\delta_{12})/p] \quad (30)$$

and the interspecies coupling is given by a formula completely similar to Eq. (25):

$$g_{12} = -2/(ma_{12}). \quad (31)$$

It is worth noting that scattering states vanish when $p \rightarrow 0$, i.e., when the magnons' momenta tend to the dispersion minima $k_1 \rightarrow Q, k_2 \rightarrow -Q$. This is a consequence of fermionization at low densities and indicates that different “species” in fact form a *single Fermi sea* at low energies. The existence of a single Fermi sea is the reason for the absence of a magnetization cusp at the transition between the vector chiral and TLL2 phases.⁴⁸ It is worth noting that a similar phenomenon is known in the one-dimensional Hubbard model: in the limit of low electron density the electrons with different spin form a common Fermi sea.⁴⁹

The resulting coupling constants for $S = \frac{1}{2}$ chain are shown in Fig. 4. One can see that on the antiferromagnetic side ($J_1 > 0$) the scattering length a_{11} is typically small (of the order of the lattice constant) and goes through zero (i.e., g_{11} has a simple pole). Similarly, on the ferromagnetic side there is a pole in g_{12} . In the previous section, we have seen that if the condition Eq. (15) is

not satisfied, a mapping to the effective continuum model of the Lieb-Liniger type (with contact interactions) is problematic. In relation to that, we would like to discuss the scattering length for an unfrustrated ($J_2 = J_2^z = 0$) spin- $\frac{1}{2}$ XXZ chain, which shows a similar behavior. Setting $J_1 = 1$, one can write the analytical expression for this scattering length as

$$a_{XXZ} = J_1^z / (1 + J_1^z). \quad (32)$$

Close to the ferromagnetic point $J_1^z = -1$, it shows resonant behavior and this allows one to develop the effective Lieb-Liniger model as the continuum limit in this region.⁵⁰ At $J_1^z = 0$, however, a_{XXZ} goes through zero and this can be interpreted as follows: the continuum limit of the XXZ spin- $\frac{1}{2}$ chain for $J_1^z > 0$ does not fit into the description in terms of the repulsive Lieb-Liniger model, rather, it is a super Tonks gas (sTG)⁵¹ with the Luttinger parameter $K < 1$. Including now the second neighbor interaction J_2^z (but not the hopping J_2), one obtains that at $J_1^z \rightarrow \infty$ and $J_2^z \rightarrow \infty$, the scattering length goes to 2. Thus, it seems that in the regime of strong coupling $|g|m \gg 1$ the scattering length has a different physical meaning, namely it can be interpreted as the excluded volume of a particle. What is the correct continuum limit in this case, however, remains a complicated issue.

IV. ANALYTICAL PREDICTIONS FOR FRUSTRATED SPIN- S CHAINS

The formalism developed in Sect. II is rather general and applies to any lattice Bose gas with degenerate inequivalent dispersion minima. Let us look in more detail at the predictions of our theory for the frustrated spin chain model defined by the Hamiltonian (1).

Figures 4-5 show the values of the “bare couplings” g_{11} and g_{12} for frustrated spin- S chains with isotropic interactions (i.e., $J_1^z = J_1$, $J_2^z = J_2$) with $S = \frac{1}{2}$, 1, and $\frac{3}{2}$ as functions of the frustration parameter $\beta = J_1/J_2$. One can see that even for the lowest spin values $S = \frac{1}{2}$ and 1, there is an excellent agreement between the approach based on the regularized Bethe-Salpeter equation and the results extracted from the direct solution of the two-magnon scattering problem.

A. Ferromagnetic frustrated isotropic chains ($J_1 < 0$, $\Delta = 1$)

On the ferromagnetic side ($\beta < 0$) the intraspecies coupling g_{11} remains small enough for its interpretation as the bare coupling of the effective continuum Lieb-Liniger model to be justified (strictly speaking, this is true for $S \geq 1$ where $|g_{11}|m \ll 1$, while for $S = \frac{1}{2}$ the coupling values are higher, $|g_{11}|m \lesssim 0.5$). For $S = \frac{1}{2}$, this coupling remains negative in the entire range of $-4 < \beta < 0$,

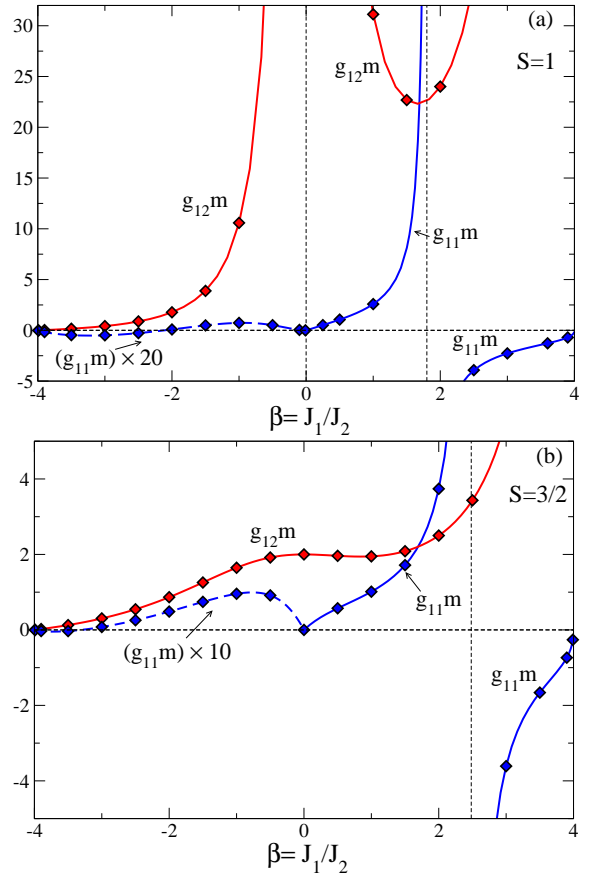


FIG. 5. (Color online). Bare coupling constants for isotropic frustrated spin chains with (a) $S = 1$ and (b) $S = \frac{3}{2}$: solid lines correspond to the calculation based on the regularized Bethe-Salpeter equation, while symbols show the results extracted from the solution of two-magnon scattering problem.

which indicates the presence of bound states and is consistent with known numerical results.^{6,7,52}

For $S = 1$, the intraspecies coupling g_{11} becomes negative in the region $-4 < \beta < \beta_f \simeq -2.11$ (see Fig. 5a), which signals the appearance of bound magnon states. As shown previously in Ref. 22 by means of an $1/S$ expansion and numerical analysis, this also leads to metamagnetism (a finite jump in the magnetization at the saturation field). The finite value of this jump can be understood in our approach by noticing the fact that the full renormalized effective coupling $\Gamma_{11}^{\Lambda*}$ depends on the particle density $n = 1 - M$, where M is the magnetization in units of saturation, and for $\beta < \beta_f$ the coupling $\Gamma_{11}^{\Lambda*}$ becomes positive at M below some critical value which determines the magnitude of the jump in M that is necessary to make the system stable again. The values of M that are spanned by the jump correspond to states with magnons collapsed into a single “drop”. Such states have negative magnetic susceptibility and are avoided in the “grand canonical” setup when one fixes the external magnetic field H .

The numerical results of Ref. 22 also suggest that the

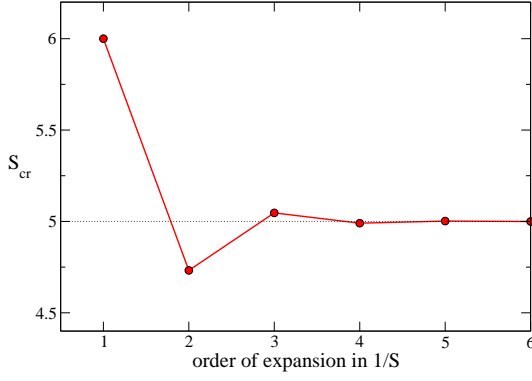


FIG. 6. (Color online). The critical value S_{cr} of the spin that marks the disappearance of the metamagnetic phase, as a function of the order n of expansion in $1/S$. The exact value is $S_{\text{cr}} = 5$, while the leading-term calculation presented in Ref. 22 gives $S_{\text{cr}} = 6$.

collapsed state has a finite vector chirality. This is easy to understand by observing that the interspecies interaction remains repulsive in the entire ferromagnetic region $-4 < \beta < 0$. Thus, it is energetically favorable to form a “drop” involving only one magnon species. As a side note, in this case g_{11} can be directly interpreted as the bare coupling of the effective continuum theory, even though the interspecies coupling g_{12} remains large $|g_{12}|m \gtrsim 1$. This can be done because the system is effectively in a one-component state.

Frustrated ferromagnetic chains with spins up to $S = \frac{9}{2}$ behave qualitatively in the same way as described above for $S = 1$. The interspecies “bare coupling” g_{12} goes through a simple pole only for $S = \frac{1}{2}$ (for $S = 1$ it goes through the pole of order 2 at $\beta = 0$), so for $S \geq 1$ it becomes positive everywhere (see Figs. 4-5,7). The intraspecies coupling g_{11} remains small and vanishes at $\beta = \beta_f$. Upon increasing S , the transition point β_f quickly moves very close to $\beta = -4$ and disappears for $S \geq 5$. This is clear from the behavior of g_{11} at $\beta \rightarrow -4$:

$$g_{11} = \frac{S-5}{4(S+1)}(\beta+4)^2 + O((\beta+4)^{5/2}). \quad (33)$$

Thus, $S_{\text{cr}} = 5$ is the critical value of spin where the metamagnetic behavior vanishes in isotropic chains (for $S > 5$, it exists only in the presence of an easy-axis anisotropy). We would like to note that Ref. 22 reported a slightly different value of $S_{\text{cr}} = 6$; this discrepancy is due to the fact that Ref. 22 used just the leading term in the large- S expansion, while our present approach is exact to all orders in $1/S$. Figure 6 illustrates the behavior of S_{cr} as a function of the order of the $1/S$ expansion.

B. Antiferromagnetic frustrated isotropic chains ($J_1 > 0$, $\Delta = 1$)

On the antiferromagnetic side $0 < \beta < 4$, the prominent feature of isotropic chains is that for realistic (low)

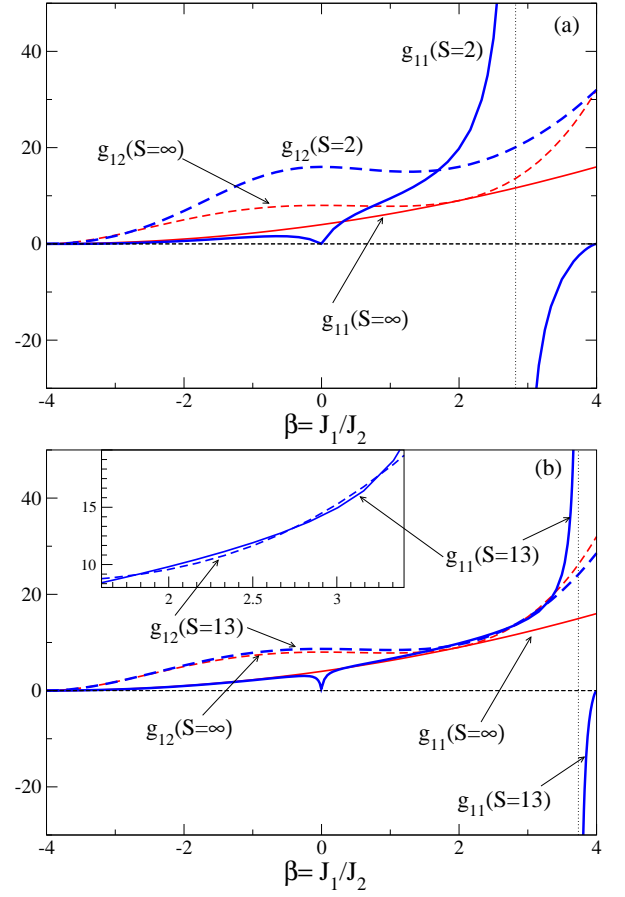


FIG. 7. (Color online). Typical behavior of the “bare couplings” g_{11} and g_{12} for isotropic spin chains with small and large spin S as functions of the frustration parameter β , compared to the semiclassical, $S \rightarrow \infty$ result (shown with thin solid line for g_{11} and thin dashed line for g_{12}): (a) for small S , there is a single crossing of g_{11} and g_{12} curves, while (b) for large $S \geq 12$, those curves cross three times (see the inset).

values of the spin S the condition Eq. (15) is not satisfied, as can be seen from Figs. 4-5. Moreover, g_{11} changes its sign through a pole in this interval of β , for any value of S . As discussed above, in this regime the system cannot be mapped to an effective continuum Lieb-Liniger-type model; however, a mapping to the effective classical Gross-Pitaevskii model (10) is still possible, and the corresponding effective couplings Γ_{11} and Γ_{12} remain positive in the entire antiferromagnetic region. For large S , the mass $m \propto S^{-1}$ becomes small (except near the two Lifshitz points $\beta = \pm 4$) which ensures that in the limit $S \rightarrow \infty$ the condition Eq. (15) is again satisfied everywhere except for small regions around the pole and the antiferromagnetic Lifshitz point.

Figure 7 shows the typical behavior of the “bare couplings” g_{11} and g_{12} for isotropic spin chains with small and large spin S , compared to the semiclassical $S \rightarrow \infty$ result. In the $S \rightarrow \infty$ limit, $g_{12} \geq g_{11}$ everywhere, and $g_{12} = g_{11}$ only at two points $\beta = -4$ (the ferromagnetic Lifshitz point) and $\beta = 2$ (the Majumdar-Ghosh

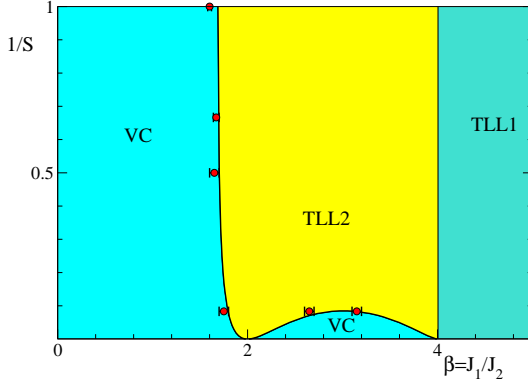


FIG. 8. (Color online). Phases of isotropic frustrated antiferromagnetic ($J_1 > 0$) spin- S chains just below the saturation field, as predicted by our effective two-component Bose gas theory. The region $\beta > 4$ corresponds to a one-component TL liquid phase (TLL1). If one varies β at fixed S , there is a single transition between the two-component TL liquid (TLL2) and the vector chiral (VC) phase for $S < 12$, while for $S \geq 12$ one encounters three consecutive TLL2-VC transitions. Symbols correspond to the transition points extracted from our numerical analysis of chirality correlators, see Section V for details.

S	1/2	1	3/2	2	12
$\beta_{\text{TLL2-VC}}$	1.682	1.688	1.694	1.702	1.80, 2.89, 3.13

TABLE I. Critical values of the exchange coupling $\beta = J_1/J_2$ for the transition from the VC to the TLL2 phase in isotropic frustrated antiferromagnetic chains of spin S at the saturation field, from the dilute Bose gas theory of the present work (cf. Figure 8).

point).⁴³ For small S , there is only one crossing of g_{11} and g_{12} at some $\beta = \beta_1 < 2$, indicating a transition between the VC phase that exists in the interval $0 < \beta < \beta_1$ and the TLL2 phase that occupies the region $\beta_1 < \beta < 4$. With increasing S , the transition point β_1 moves toward the Majumdar-Ghosh point $\beta = 2$, see Fig. 8 and Table I. For very large $S \geq 12$, two more crossings of the g_{11} and g_{12} curves appear (see the inset in Fig. 7b), and another piece of the VC phase emerges in the region $2 < \beta < 4$, filling it completely as S goes to infinity (see Fig. 8).

C. Anisotropic chains ($\Delta \neq 1$)

Motivated by the availability of numerical results¹⁴ for anisotropic frustrated ferromagnetic chains with $S = 1/2$, we would like to check our theoretical predictions for anisotropic systems as well. Figure 9 shows the behavior of the “bare couplings” for $S = \frac{1}{2}$ anisotropic chains with two different values of $\beta < 0$, as functions of the anisotropy $J_1^z/J_1 = J_2^z/J_2 = \Delta$. For $\beta = -0.3$, the intraspecies coupling g_{11} remains small and vanishes at $\Delta \simeq 0.56$, while g_{12} is negative and large ($|g_{12}|m \gtrsim 1$). This indicates a transition from the vector chiral phase at

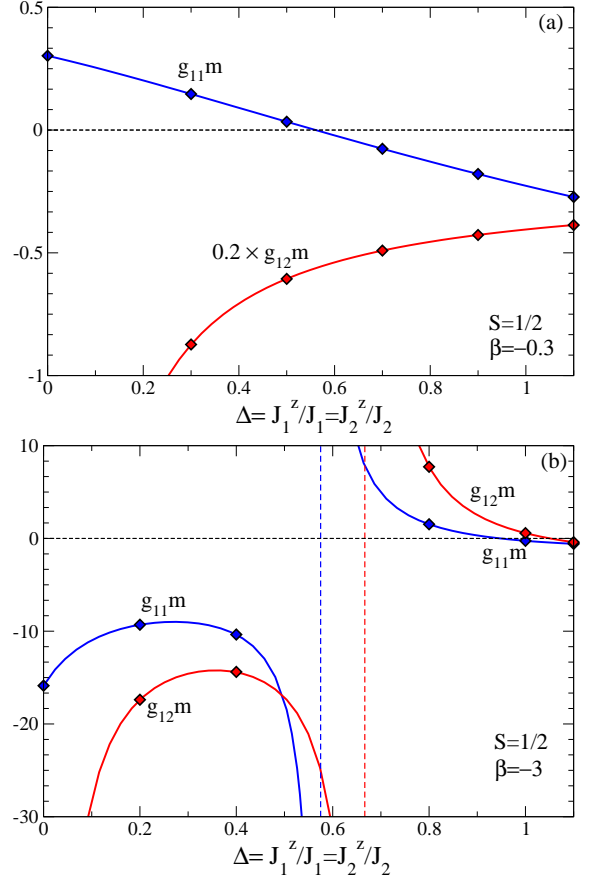


FIG. 9. (Color online). Bare coupling constants for $S = \frac{1}{2}$ anisotropic chain with $J_1^z/J_1 = J_2^z/J_2 = \Delta$: (a) $J_1/J_2 = -0.3$ and (b) $J_1/J_2 = -3.0$.

$\Delta < 0.56$ to a phase with bound states at $\Delta > 0.56$. This agrees favorably with the numerical results of Ref. 14 that reports a transition between the chiral and nematic phases at $\Delta \simeq 0.6$.

For $\beta = -3$, there is a crossing of g_{11} and g_{12} at $\Delta \simeq 0.5$ (see Fig. 9b) that indicates a transition between the TLL2 phase at $\Delta < 0.5$ and the VC phase at $\Delta > 0.5$, nicely fitting to the numerical data of Ref. 14. Both g_{11} and g_{12} go through poles and become positive (which does not change the phase since in the course of this change one always has $\Gamma_{12} > \Gamma_{11}$), then they become small and positive around $\Delta = 1$, and g_{11} crosses zero at $\Delta \simeq 0.947$, indicating a transition from the VC phase to a phase with bound states (g_{12} changes its sign later, at about $\Delta = 1.05$). Again, this is in good agreement with the numerical study Ref. 14 that observes a transition around $\Delta = 0.95$.

Figure 10 shows the predicted phase diagram of anisotropic $S = \frac{1}{2}$ and $S = 1$ chains immediately below the saturation field in the (β, Δ) plane. One can see that with increasing S the TLL2 phase shrinks and the phase with bound states is pushed toward higher Δ (for $S > 5$ it lies entirely in the easy-axis region $\Delta > 1$). The vector chiral phase dominates the phase diagram. One

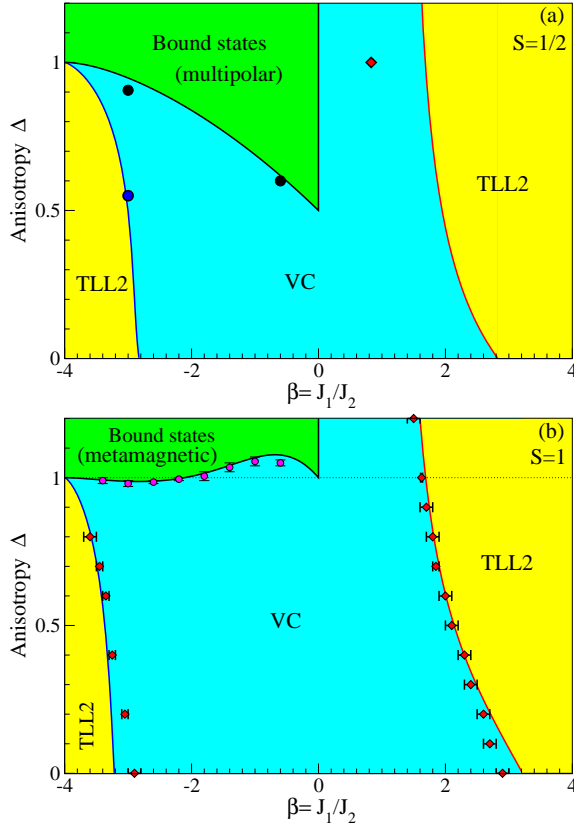


FIG. 10. (Color online). Phase diagrams of anisotropic ($J_1^z/J_1 = J_2^z/J_2 = \Delta$) frustrated chains with (a) $S = \frac{1}{2}$ and (b) $S = 1$ right below the saturation field, derived from our dilute Bose gas approach. The boundary between the two-component Tomonaga-Luttinger liquid (TLL2) and the vector chiral (VC) phases has been extracted from the condition $g_{11} = g_{12}$. At the boundary of the region labeled “Bound states” the intraspecies coupling g_{11} changes its sign from positive to negative (it turns out that g_{11} always becomes negative before g_{12} does). The “bound states” region for $S = \frac{1}{2}$ in fact contains multiple phases corresponding to bound states of a different number of magnons,^{6,7} which is beyond the scope of the present theory that can only detect the presence of two-magnon bound states. For $S = 1$, the “bound states” region is metamagnetic,²² i.e., it exhibits a finite magnetization jump immediately below the saturation field. For $S = \frac{1}{2}$, circles correspond to the numerical data of Ref. 14, and the diamond is the location of the VC-TLL2 transition at $\Delta = 1$ as found numerically in Refs. 11 and 12. For $S = 1$, symbols denote our DMRG results (see Section V for details): diamonds and circles denote the phase transition points extracted from the analysis of the chirality correlators and the magnetization curves, respectively.

can conclude that the present theory reliably detects the transition points in anisotropic ferromagnetic chains even at such low values of the spin as $S = \frac{1}{2}$. It is worth noting that the transition point between the TLL2 and VC phases in the $\beta = -3$, $S = \frac{1}{2}$ chain comes out correctly despite the fact that both $|g_{12}|m$ and $|g_{11}|m$ are large at the transition. On the antiferromagnetic side,

the only numerical data available in the literature is for the isotropic $S = \frac{1}{2}$ chain.^{11,12} In this case, for a reason that is not yet clear, the agreement between the theory and numerics is considerably worse.

V. NUMERICAL ANALYSIS

To verify our theoretical predictions, we have performed extensive density matrix renormalization group (DMRG) simulations. For a detailed description of the DMRG technique,²⁶ we refer the reader to the review Ref. 27. We focus on two quantities: First, we calculate the central charge from the scaling behavior of the von Neumann entropy, which allows us to distinguish one- from two-component phases. Second, we compute the vector chirality order parameter from the analysis of chiral correlation functions, to identify those one-component phases that have long-range vector chiral order. The goal is to provide a numerical check of the phase diagrams for isotropic and anisotropic frustrated chains, Figs. 8 and 10, respectively. In order to identify the region with bound states in anisotropic chains, we calculate magnetization curves. We have studied systems of different sizes L ranging from $L = 50$ to $L = 400$, both with periodic and open boundary conditions, typically keeping 600 to 1500 states in most calculations.

A. Central charge

Our theory suggests that close to the saturation field, in antiferromagnetic frustrated chains with spin values of $1/2 < S < 12$, one encounters two phase transitions when increasing β from zero: (i) from the VC phase into the TLL2 phase and (ii) from the TLL2 phase into the TLL1 phase (compare Fig. 8). The TLL2 phase has central charge $c = 2$, while the VC and the TLL1 phases have $c = 1$, suggesting that a calculation of c can be helpful in determining the phase boundaries.

To accomplish that, we exploit that the von Neumann entropy S_{vN} can be obtained as a by-product of any DMRG calculation. Furthermore, from the finite-size scaling of S_{vN} , one can extract the central charge. The von-Neumann entropy is defined as

$$S_{vN,L}(l) = -\text{tr}(\rho_l \ln \rho_l), \quad (34)$$

where ρ_l is the reduced density matrix for a subsystem of length l embedded in a chain of a finite length L . In a gapless state that is conformally invariant, the l and L dependence of the von Neumann entropy is given by^{53,54}

$$S_{vN,L}(l) = \frac{c}{3} \ln \left[\frac{L}{\pi} \sin \left(\frac{\pi}{L} l \right) \right] + g, \quad (35)$$

which is valid for systems with periodic boundary conditions (PBC). Here g is a non-universal constant that

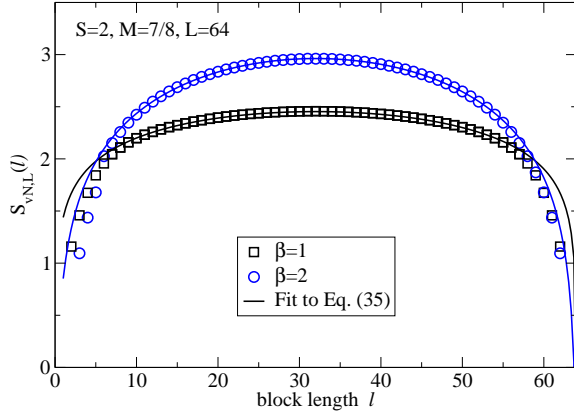


FIG. 11. (Color online). The von Neumann entropy $S_{vN,L}(l)$ vs block length l for $S = 2$ at $M = 7/8$ for $\beta = 2$ (circles) and $\beta = 1$ (squares). The solid lines are fits to Eq. (35), resulting in $c \approx 1.01$ and $c = 2.10$, respectively (the last 10 data points were excluded from the fits). Symbols are DMRG data for $m = 1500$ states.

depends on the magnetization M . As DMRG directly accesses the eigenvalues of these reduced density matrices,^{26,27} it is straightforward to measure $S_{vN,L/2}(l)$ with this method. In the case of open boundary conditions (OBC), the von Neumann entropy is given by one half of the formula Eq. (35), where besides g , there are also contribution that oscillates as a function of l .

Typical DMRG results for the von Neumann entropy of chains with $L = 64$ spins and PBC are presented in Fig. 11 for $S = 2$, together with a fit of Eq. (35) to the numerical data (lines). These fits result in $c \approx 1$ for $\beta = 1$ and $c \approx 2.1$ for $\beta = 2$ at $M = 7/8$. As it turns out, there are strong finite-size effects in the estimation of c from fits to Eq. (35), in particular at high fields close to saturation which are our primary interest. Nishimoto⁵⁵ has recently suggested to calculate c from the following formula:

$$c = \frac{3[S_{vN,L}(L/2 - 1) - S_{vN,L}(L/2)]}{\ln[\cos(\pi/L)]}, \quad (36)$$

which turns out to converge much faster with the system size. However, the numerical data needs to be sufficiently accurate for Eq. (36) to yield reliable results, and we found that one has to push the number of states in a typical DMRG calculation to about $m \sim 1500$ to achieve good accuracy. For instance, for the parameter of Fig. 11, Eq. (36) results in $c = 1.005$ for $\beta = 1$. We used Eq. (36) to extract c whenever the DMRG calculation proved to be sufficiently accurate, and resorted to fits to Eq. (35) (or its OBC counterpart) otherwise.

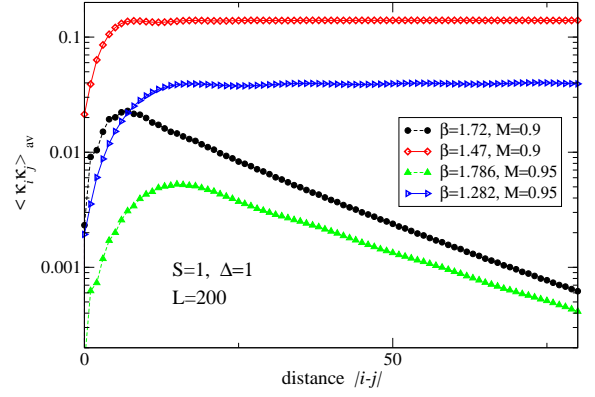


FIG. 12. (Color online). Typical vector chirality correlation functions for an isotropic $S = 1$ chain of $L = 200$ spins.

B. Chirality order parameter

To study the behavior of the vector chirality, we have calculated correlators of the form

$$\langle \kappa_i \kappa_j \rangle, \quad \kappa_i = [\mathbf{S}_i \times \mathbf{S}_{i+1}]^z. \quad (37)$$

The chiral order parameter κ has been extracted as

$$\kappa^2 = \lim_{|i-j| \gg 1} \langle \kappa_i \kappa_j \rangle_{av}, \quad (38)$$

where the index “av” means that correlators were averaged over pairs of sites (i, j) with the same $|i - j|$, while care was taken to stay “in the bulk”, i.e., i and j were kept sufficiently far away from the ends of the chain. Figure 12 shows typical vector chirality correlation functions for a $S = 1$ isotropic frustrated chain of length $L = 200$.

C. Numerical results: Isotropic chains

Our results for the central charge of isotropic frustrated chains are shown in Fig. 13. We have collected data at fixed magnetization M for $S = 1, \frac{3}{2}, 2$. From the figure we clearly identify two phase transitions: (i) at a critical, S -dependent $\beta \gtrsim 3$ from TLL1 ($c = 1$) phase into the TLL2 phase ($c = 2$) and (ii) at $\beta \gtrsim 1.6$, from the TLL2 phase into another $c = 1$ phase. Based on our theory, we expect this latter phase to have vector chiral order (which is verified by calculating the chiral order parameter, see below).

The position of the phase transition from TLL2 into VC depends only weakly on S , consistent with our theory (compare the values given in Tab. I). According to our theory, the phase transition from TLL1 into TLL2 happens at approximately $\beta = 4$, the Lifshitz point, in the limit of $M \rightarrow 1$. Our numerical data for $M < 1$, however, shows that this transition sets in at a slightly smaller $\beta \lesssim 3.5$ than what one would expect from Fig. 8. This suggests that the phase boundary depends on M . Indeed, for instance, in the case of $S = 1$, this phase

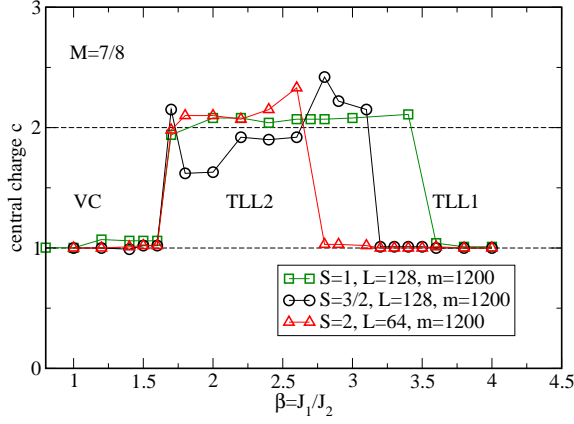


FIG. 13. (Color online). Central charge at $M = 7/8$ for $S = 1, 3/2$, and 2 , as extracted from Eq. (36) [The data points in the $c \sim 2$ region, i.e., $1.5 < \beta < 2.5$ were extracted from direct fits of Eq. (35) to the DMRG results for $S_{vN,L}(l)$].

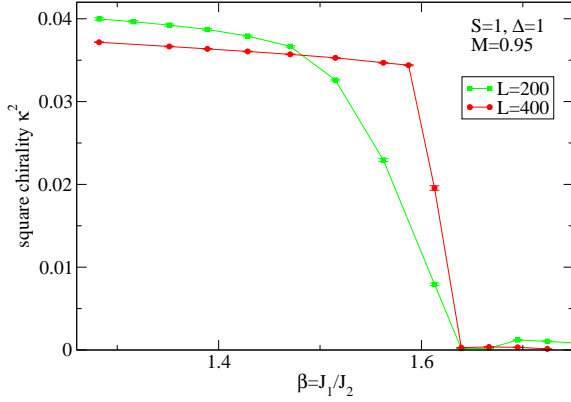


FIG. 14. (Color online). Square of the vector chirality order parameter κ^2 for frustrated isotropic antiferromagnetic $S = 1$ chain at fixed value of the magnetization $M = 95/100$, as a function of the frustration parameter $\beta = J_1/J_2$.

boundary shifts to smaller values of β as M decreases which can be deduced from the analysis of magnetization curves presented in Ref. 23, where this particular phase transition shows up as a kink in $M(H)$. We have not systematically studied the M dependence as the DMRG data for $S_{vN,L}$ tends to converge rather slowly at large M . Our numerical results for c are in very good overall agreement with the theory.

We next verify that the $c = 1$ phase at $\beta \lesssim 1.6$ is the VC phase, by directly calculating the chiral order parameter as described above; the results are shown in Figs. 14 and 15. One can clearly see from Fig. 15 that, in agreement with our analytical predictions, the transition point β from the vector chiral phase to the two-component Tomonaga-Luttinger liquid increases slowly with the increasing spin value S . Our numerical results for the transition boundaries in isotropic frustrated chains are shown as symbols in the phase diagram of Fig. 8.

Figure 14 illustrates that with the increasing system

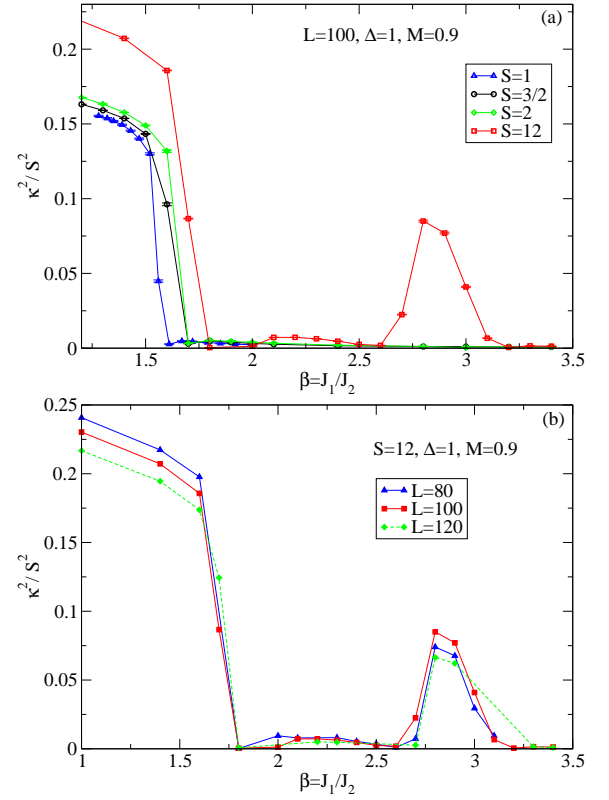


FIG. 15. (Color online). Square of the vector chirality order parameter κ^2 for frustrated isotropic antiferromagnetic spin- S chains, at fixed value of the magnetization $M = 9/10$, as a function of the frustration parameter $\beta = J_1/J_2$: (a) for chains consisting of $L = 100$ spins, at different values of S ; (b) for $S = 12$ chains of different length L .

size L , the VC-TLL2 transition becomes more steep. This is consistent with the first-order character of this transition as predicted by the theory (recall that the VC-TLL2 transition corresponds to phase separation in the language of the effective two-component Bose gas theory).

For high magnetization sectors it is possible to study large spins as well and results for $S = 12$ are included in Fig. 15. One should take those $S = 12$ results with some caution: our data for small systems (consisting of 80, 100, and 120 sites) still show strong nontrivial size dependence (see Fig. 15b) that precludes infinite-size extrapolation, and we could not study larger systems because of the rapidly growing dimension of the Hilbert space. Nevertheless, the resulting picture for $S = 12$ qualitatively agrees with our analytical prediction, namely, one can see the recurring TLL2-VC phase transitions in accordance with the phase diagram of Fig. 8.

D. Numerical results: Anisotropic $S = 1$ chain

We have studied numerically the phase diagram of the anisotropic ($J_2^z/J_2 = J_1^z/J_1 = \Delta$) frustrated spin-

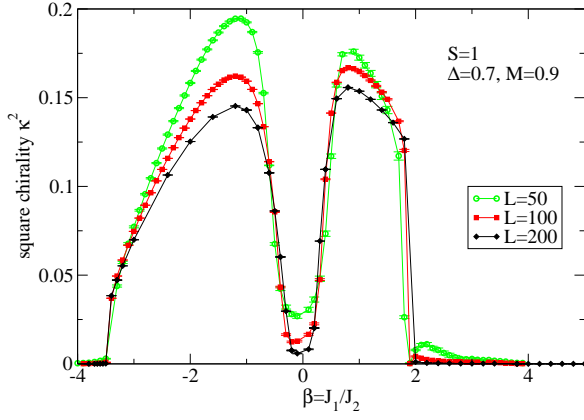


FIG. 16. Square of the vector chirality order parameter κ^2 for frustrated antiferromagnetic $S = 1$ chain for $\Delta = 0.7$, at fixed value of the magnetization $M = 9/10$, as a function of the frustration parameter $\beta = J_1/J_2$.

1 chain, to verify the analytically predicted phase diagram of Fig. 10b. Figure 16 shows the typical dependence of the chiral order parameter κ on the frustration parameter β for anisotropic $S = 1$ chain, at fixed anisotropy Δ and magnetization M , for three different system sizes. One can notice that finite-size effects are not always monotonous, which complicates the extrapolation to infinite system size.

In Fig. 17, we present our results for the dependence of the central charge on β , for the same parameters as used for the chirality in Fig. 16. These data were obtained from systems with open boundary conditions for which we could obtain reliable data. The additional oscillatory contributions to S_{vN} are evident from the inset of Fig. 16. The behavior of the central charge is consistent with the results for the chirality: Whenever $\kappa^2 > 0$, $c = 1$. At both $\beta > 2$ and $\beta \lesssim -3.5$, where κ drops to zero, the central charge goes up to $c = 2$, indicating phase transition from VC to TLL2 phase.

As for the regime of almost decoupled chains $|\beta| \ll 1$, one should keep in mind that this is a particularly difficult parameter region for DMRG calculations, and the apparent deviation from the analytical predictions (according to which $c = 2$ is only realized for one point $\beta = 0$) is an artefact of the rapidly deteriorating accuracy at $\beta \rightarrow 0$.

In order to study the phase boundary between the VC and “bound states” (metamagnetic) phase, we have also calculated magnetization curves, and looked at the value ΔS^z of the steps by which the magnetization changes. While inside the VC phase (where magnons interact repulsively) the magnetization grows in steps of $\Delta S^z = 1$ when increasing the magnetic field, after crossing the metamagnetic region boundary the height of steps in the magnetization curves quickly changes to higher values $\Delta S^z = 2, 3$, etc. Typical results for $M(H)$ are shown in Fig. 18. In this example ($S = 1$, $\beta = -1.2$), we see metamagnetic behavior (a jump in $M(H)$) directly un-

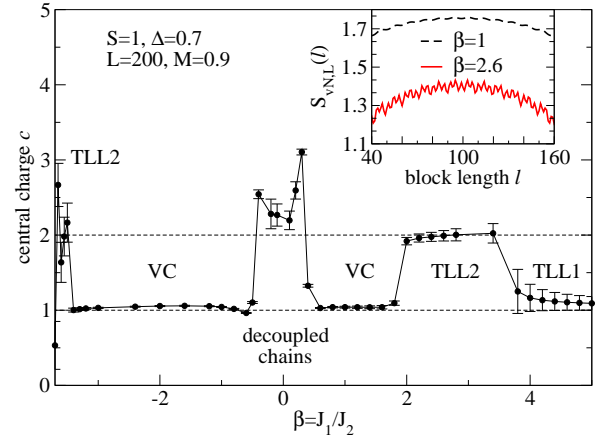


FIG. 17. Main panel: Central charge, obtained with open boundary conditions, for a frustrated antiferromagnetic $S = 1$ chain for $\Delta = 0.7$, at magnetization $M = 9/10$, as a function of the frustration parameter $\beta = J_1/J_2$. Inset: von Neumann entropy $S_{vN,L}(l)$ versus l at $\beta = 1, 2.6$.

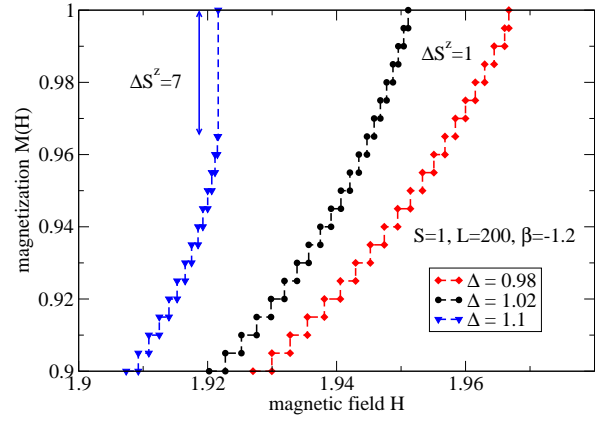


FIG. 18. Typical magnetization curves for $S = 1$ chain with $\beta = -1.2$, at different values of the anisotropy Δ . For $\Delta = 1.1$, the curve exhibits a metamagnetic jump at the saturation field (similar jump for $\Delta = 1$, for $-4 < \beta < -2.11$ has been already discussed in Ref.²²).

der saturation magnetization for $\Delta = 1.1$, but not for $\Delta = 1.02$ or $\Delta = 0.98$. The results for the onset of the metamagnetic behavior as a function of Δ and β are included in Fig. 10(b) (circles).

Our numerical results for the TLL2-VC phase boundary are shown by symbols in Fig. 10b. The overall agreement between the theory and numerics is very good.

VI. SUMMARY

We have developed the effective theory for low-density one-dimensional lattice Bose gas with two degenerate dispersion minima. This study has been motivated by the problem of the ground state phase transitions in frustrated spin- S chains subject to strong magnetic fields just

slightly lower than the saturation field, where such a system can be viewed as a dilute lattice gas of magnons in the fully polarized background. At low density of magnons they can be treated as bosonic particles, and in a wide region of parameters the magnon dispersion has two degenerate minima at inequivalent points $\pm Q$ in the momentum space.

The low-energy effective theory has the form of the Gross-Pitaevskii functional for a two-component field. We have developed the scheme that allows the calculation of renormalized effective interactions Γ_{11} , Γ_{12} . Applying this formalism to frustrated spin- S chains, we establish the magnetic phase diagram of isotropic and anisotropic, ferro- and antiferromagnetic frustrated chains close to saturation and study phase transitions between several nontrivial states, including the two-component Tomonaga-Luttinger liquid (TLL2), vector chiral (VC) phase, and phases with bound magnons. Our scheme does not involve an $1/S$ expansion, and thus allows us to draw quantitative predictions for arbitrary spin.

We complement our analytical predictions by a variety of numerical results obtained by means of the density matrix renormalization group technique. Particularly, we compute the central charge as a function of the frustration parameter close to saturation which allows us to locate phase transitions between one- and two-component states. Further, we directly compute chirality correlators in order to identify those one-component states that have vector chiral order. In addition, we study the magnetization curves to detect the presence of magnon bound states. These numerical results are in a good quantitative agreement with our theoretical predictions for chains of spin $S \geq 1$. At the same time, in the case of frustrated antiferromagnetic $S = \frac{1}{2}$ chains, the quantitative discrepancy between our theoretical prediction and the numerical results by Okunishi¹¹ and Hikiara *et al.*¹² for the location of the TLL2/VC phase boundary is unexpectedly large. Nevertheless, even for $S = \frac{1}{2}$ our theory still correctly captures the topology of the phase diagram.

ACKNOWLEDGMENTS

We thank H. Frahm for useful discussions. A.K. gratefully acknowledges the hospitality of the Institute for Theoretical Physics at the Leibniz University of Hannover. This work has been supported by the cluster of excellence QUEST (Center for Quantum Engineering and Space-Time Research). T.V. acknowledges SCOPES Grant IZ73Z0-128058.

Appendix A: Low-energy effective theory and connection to the two-component Lieb-Liniger model

To obtain the low-energy effective theory for the Hamiltonian (5), we define the bosonic field $\psi =$

$\sum_k b_k e^{ikx}$ with the Euclidean action given by $\mathcal{A}_\psi = \int d\tau \left\{ \int dx \psi^* \partial_\tau \psi + \mathcal{H}[\psi] \right\}$, and divide the field ψ into “slow” parts $\Phi^{1,2}$ and the “fast” part ϕ :

$$\psi = \sum_{\alpha=1,2} \Phi^\alpha e^{i\sigma_\alpha Qx} + \phi, \quad (\text{A1})$$

$$\Phi^\alpha = \sum_{|k| < \Lambda} b_{\sigma_\alpha Q + k} e^{ikx}, \quad \sigma_\alpha = \begin{cases} 1, & \alpha = 1 \\ -1, & \alpha = 2 \end{cases},$$

where Λ is the running cutoff. Treating the “slow” part as the background field, one can integrate over the fast modes $\int \mathcal{D}[\phi] e^{-\mathcal{A}_\psi} = e^{-\mathcal{A}_\Phi}$ and obtain the effective action \mathcal{A}_Φ that is essentially the generating functional of vertex functions⁵⁶ and can be written as follows:

$$\begin{aligned} \mathcal{A}_\Phi &= \Phi_{k,\omega}^{\alpha,*} U_{k,\omega}^{(2),\alpha\beta} \Phi_{k,\omega}^\beta \\ &+ \frac{1}{2} \Phi_{k+q,\Omega+\omega}^{\alpha,*} \Phi_{k'-q,\Omega'-\omega}^{\beta,*} U_{q,k,k',\Omega+\Omega'}^{(4),\alpha\beta} \Phi_{k,\Omega}^\alpha \Phi_{k',\Omega'}^\beta \\ &+ (\text{higher-order terms in } \Phi). \end{aligned} \quad (\text{A2})$$

In the above equation, the summation over repeated indices is implied, and the Λ -dependent coefficients $U^{(n)}$ can be expressed through the vertex functions $\Gamma^{(n)}$ of the initial theory determined by the action \mathcal{A}_ψ :

$$\begin{aligned} U_{k,\omega}^{(2),\alpha\beta} &= \delta_{\alpha\beta} \Gamma^{(2)}(\sigma_\alpha Q + k, \omega), \\ U_{q,k,k',\omega}^{(4),\alpha=\beta} &= \Gamma_q^{(4)}(\sigma_\alpha Q + k, \sigma_\alpha Q + k'; \omega), \\ U_{q,k,k',\omega}^{(4),\alpha \neq \beta} &= \Gamma_q^{(4)}(\sigma_\alpha Q + k, \sigma_\beta Q + k'; \omega) \\ &+ \Gamma_{(\sigma_\beta - \sigma_\alpha)Q + k' - k - q}^{(4)}(\sigma_\alpha Q + k, \sigma_\beta Q + k'; \omega), \end{aligned} \quad (\text{A3})$$

with the restriction that sums in the internal lines of the corresponding Feynman diagrams include only “fast” modes with momenta p outside the regions $|p \pm Q| < \Lambda$.

The two-point function $-\Gamma^{(2)}(k, \omega)$ is equal to the Green function $G(k, \omega)$. In the limit $\mu \rightarrow 0$, i.e., in the absence of particles, the self-energy vanishes³⁰ and the full propagator $G(k, \omega)$ is given by its bare value $G^{(0)}(k, \omega) = (i\omega - \varepsilon_k)^{-1}$. The four-point vertex $\Gamma_q^{(4)}(k, k', \omega) \equiv \Gamma_q^\Lambda(k, k'; E = i\omega)$ is determined by the Bethe-Salpeter equation, which in the limit $\mu \rightarrow 0$ takes the simple form of Eq. (9), with the infrared cutoff Λ around the momenta $\pm Q$ introduced into the integral.

We neglect higher-order terms in the expansion (A2), which is justified at low densities, replace $\varepsilon_{\pm Q+k}$ that enters $U^{(2)}$ by its leading small- k term $k^2/(2m)$, and neglect the momentum and energy dependence of $U^{(4)}$, which is appropriate in the limit of small Λ . Then the effective low-energy action (A2) takes the form of the Gross-Pitaevskii functional for a two-component field:

$$\begin{aligned} \mathcal{A}_\Phi &= \int d\tau \int dx \left\{ \Phi^{\alpha*} (\partial_\tau - \mu) \Phi^\alpha \right. \\ &\quad \left. + \frac{1}{2m} |\partial_x \Phi^\alpha|^2 + \frac{1}{2} \Phi^{\alpha*} \Phi^{\beta*} \Gamma_{\alpha\beta}^\Lambda \Phi^\alpha \Phi^\beta \right\}, \end{aligned} \quad (\text{A4})$$

where the renormalized running couplings are given by $\Gamma_{\alpha\beta}^\Lambda = U_{0,0,0,0}^{(4),\alpha\beta}$. As shown in the main text by solving the

BS equation, in the one-dimensional case the dependence of those couplings on the cutoff has the form

$$\Gamma_{\alpha\beta}^\Lambda = \pi\Lambda/m + C_{\alpha\beta}\Lambda^2 + \dots, \quad \Lambda \rightarrow 0. \quad (\text{A5})$$

Now, consider the system of two bosonic species $\varphi_{1,2}$ interacting via contact potential, described by the action

$$\begin{aligned} \mathcal{A}_\varphi = \int d\tau \int dx \Big\{ & \varphi_\alpha^* (\partial_\tau - \frac{\partial_x^2}{2m} - \mu) \varphi_\alpha \\ & + \frac{1}{2} g_{\alpha\beta} n_\alpha(x) n_\beta(x) \Big\}, \end{aligned} \quad (\text{A6})$$

where $n_\alpha = |\varphi_\alpha|^2$, $\alpha = 1, 2$ are the densities of the two components. This is nothing but the two-component Lieb-Liniger model. The low-energy effective theory for this model can be again cast in the form (A4),⁴² with the renormalized couplings given by

$$\Gamma_{\alpha\beta}^{(LL)} = \frac{g_{\alpha\beta}}{1 + \frac{m}{\pi\Lambda} g_{\alpha\beta}} = \frac{\pi\Lambda}{m} - \frac{1}{g_{\alpha\beta}} \left(\frac{\pi\Lambda}{m} \right)^2 + \dots, \quad \Lambda \rightarrow 0. \quad (\text{A7})$$

Comparing (A7) and (A5), one can establish a correspondence between the original lattice problem (5) and the simplified continuum model (A6) of the Lieb-Liniger type, that is characterized by bare couplings $g_{\alpha\beta}$.

Appendix B: Symmetrized equations for Γ_{11} , Γ_{12}

To simplify the equation (9), we first symmetrize the kernel. Let us introduce the following functions that are even in the transferred momentum q :

$$\Gamma_q^{(11)}(E) \equiv \Gamma_q(Q, Q; E), \quad (\text{B1})$$

$$\Gamma_q^{(12)}(E) \equiv \Gamma_{Q+q}(-Q, Q; E) + \Gamma_{Q-q}(-Q, Q; E),$$

then $\Gamma_{11}(E) = \Gamma_{q=0}^{(11)}$ and $\Gamma_{12}(E) = \Gamma_{q=Q}^{(12)}$. From (9), using the identities $\varepsilon_k = \varepsilon_{-k}$, $V_q(k, k') = V_{-q}(k', k)$, and

$\Gamma_q(k, k'; E) = \Gamma_{-q}(k', k; E)$, one readily obtains the following equation for $\Gamma_q^{(11)}$:

$$\begin{aligned} \Gamma_q^{(11)}(E) &= V_{11}(Q, 0) - \frac{1}{L} \sum_p \frac{V_{11}(q, p) \Gamma_p^{(11)}(E)}{\varepsilon_{Q+p} + \varepsilon_{Q-p} - E}, \\ V_{11}(q, p) &= \frac{1}{2} [V_{q-p}(Q + p, Q - p) + (p \mapsto -p)], \end{aligned} \quad (\text{B2})$$

and a similar equation for $\Gamma_q^{(12)}$:

$$\begin{aligned} \Gamma_q^{(12)}(E) &= 2V_{12}(q, Q) - \frac{1}{L} \sum_p \frac{V_{12}(q, p) \Gamma_p^{(12)}(E)}{2\varepsilon_p + E}, \\ V_{12}(q, p) &= \frac{1}{2} [V_{q-p}(p, -p) + V_{q+p}(-p, +p)]. \end{aligned} \quad (\text{B3})$$

Explicitly, the symmetrized kernels for our model are

$$\begin{aligned} V_{11}(q, p) &= \begin{cases} V^z(q, p) + U_1 \cos p + U_2 \cos 2p, & S \geq 1 \\ V^z(q, p) + U, & U \rightarrow \infty \end{cases} \quad S = \frac{1}{2}, \\ V_{12}(q, p) &= \begin{cases} V^z(q, p) - J(p), & S \geq 1 \\ V^z(q, p) + U, & U \rightarrow \infty \end{cases} \quad S = \frac{1}{2}, \end{aligned} \quad (\text{B4})$$

where

$$\begin{aligned} U_1 &= -2J_1 \cos Q, \quad U_2 = -2J_2 \cos 2Q, \\ V^z(q, p) &= 2J_1^z \cos(q) \cos(p) + 2J_2^z \cos(2q) \cos(2p) \end{aligned} \quad (\text{B5})$$

Solutions of Eqs. (B2), (B3) can be now sought in the form containing only even Fourier harmonics:

$$\begin{aligned} \Gamma_q^{(11)} &= A_1 + A_2 \cos q + A_3 \cos 2q, \\ \Gamma_q^{(12)} &= B_1 + B_2 \cos q + B_3 \cos 2q. \end{aligned} \quad (\text{B6})$$

This ansatz transforms the integral equations (B2), (B3) into 3×3 linear systems:

$$\begin{pmatrix} \tau_{11}^A + \frac{2S-1}{2S(U_1+U_2)-E} & \tau_{12}^A & \tau_{13}^A \\ \tau_{12}^A & \tau_{22}^A + \frac{1}{2J_1^z} & \tau_{23}^A \\ \tau_{13}^A & \tau_{23}^A & \tau_{33}^A + \frac{1}{2J_2^z} \end{pmatrix} \begin{pmatrix} A_1 \\ A_2 \\ A_3 \end{pmatrix} = \begin{pmatrix} 1/c_S \\ 1 \\ 1 \end{pmatrix} \quad (\text{B7})$$

$$\begin{pmatrix} \tau_{11}^B + \frac{2S-1}{2S(U_1+U_2)-E} & \tau_{12}^B & \tau_{13}^B \\ \tau_{12}^B & \tau_{22}^B + \frac{1}{2J_1^z} & \tau_{23}^B \\ \tau_{13}^B & \tau_{23}^B & \tau_{33}^B + \frac{1}{2J_2^z} \end{pmatrix} \begin{pmatrix} B_1 \\ B_2 \\ B_3 \end{pmatrix} = \begin{pmatrix} 2/c_S \\ 2 \cos Q \\ 2 \cos 2Q \end{pmatrix}, \quad (\text{B8})$$

where $c_S = 1 - \frac{E}{2S(U_1+U_2)}$ for $S \geq 1$ and $c_S = 1$ for $S = \frac{1}{2}$, and the matrix coefficients are given by

$$\tau_{ij}^A = \frac{1}{L} \sum_k \frac{f_i f_j}{\varepsilon_{Q+k} + \varepsilon_{Q-k} - E}, \quad \tau_{ij}^B = \frac{1}{L} \sum_k \frac{f_i f_j}{2\varepsilon_k - E}, \quad f_1 = 1, \quad f_2 = \cos k, \quad f_3 = \cos 2k. \quad (\text{B9})$$

The solutions of those equations can be easily obtained

in a closed though somewhat cumbersome form.

Appendix C: The continuum limit for a one-component lattice Bose gas: bare and renormalized interaction

Consider Bose gas on a lattice, with the single-particle kinetic energy ε_k that behaves quadratically at small momenta, $\varepsilon_k \simeq k^2/2m$ at $k \rightarrow 0$. Let us assume there is an on-site interaction of strength g_0 . In the limit of vanishing density, one can write down the Bethe-Salpeter equation for the renormalized two-body interaction $\Gamma_q(k=0, k'=0; E=0) \equiv \Gamma$ in the same way as we have done in Sect. II, but now it is considerably simplified since the bare interaction vertex $V_q(k, k) = g_0$ is independent of momenta, and the renormalized interaction Γ is independent of the transferred momentum q :

$$\Gamma = g_0(1 - \Gamma I), \quad I = \frac{1}{\pi} \int_{\Lambda}^{\Lambda_{UV}} \frac{dp}{2\varepsilon_p}. \quad (C1)$$

Here $\Lambda_{UV} = \pi$ is the natural ultraviolet lattice cutoff, and Λ is the running infrared cutoff. The flow eventually gets stopped at $\Lambda = \Lambda_*$ given in Eq. (17). At low gas density n the regulator $\Lambda_* = \pi n/2 \ll 1$, so we are interested in the behavior of $\Gamma(\Lambda)$ at $\Lambda \rightarrow 0$.

For the continuum Bose gas model with contact interaction of the form $U(x - x') = g_c \delta(x - x')$ (the Lieb-Liniger model), the equation for the renormalized interaction Γ_c is very similar,

$$\Gamma_c = g_c(1 - \Gamma_c I_c), \quad I_c = \frac{m}{\pi} \int_{\Lambda}^{\infty} \frac{dp}{p^2} = \frac{m}{\pi\Lambda}. \quad (C2)$$

The running coupling in the continuum model is thus given by

$$\Gamma_c = \frac{g_c}{1 + \frac{m}{\pi\Lambda} g_c}. \quad (C3)$$

Let us come back to the lattice expression (C1). Since $\varepsilon_k \rightarrow k^2/2m$ at $k \rightarrow 0$, it is easy to see that the integral I in (C1) behaves as

$$I \rightarrow \frac{m}{\pi\Lambda} + I_{\text{lat}}, \quad \Lambda \rightarrow 0, \quad (C4)$$

where I_{lat} is some parameter of the order of unity that incorporates all effects of the lattice (ultraviolet cutoff as well as the deviation of the dispersion ε_p from the quadratic law). The important point is that this constant I_{lat} , depending on the lattice details, can be *negative*: for instance, if one takes the free particle dispersion $\varepsilon_p \simeq p^2/(2m)$ and simply introduces the lattice cutoff Λ_{UV} , then $I_{\text{lat}} = -m/(\pi\Lambda_{UV})$. Curiously, this constant I_{lat} does not appear if the particle dispersion is a pure cosine (i.e., only nearest-neighbor hopping is taken into

account): it is easy to show that for $\varepsilon_p = \frac{1}{m}(1 - \cos p)$ the integral I in (C1) is

$$I = \frac{m}{2\pi \tan(\Lambda/2)} \rightarrow \frac{m}{\pi\Lambda} (1 - \frac{\Lambda^2}{12} + \dots) \quad \text{at } \Lambda \rightarrow 0, \quad (C5)$$

i.e., in this case $I_{\text{lat}} \rightarrow 0$.

The resulting behavior of the running coupling in the lattice problem can be represented in the form identical to that of the continuum model:

$$\Gamma = \frac{\tilde{g}_0}{1 + \frac{m}{\pi\Lambda} \tilde{g}_0}, \quad \tilde{g}_0 = \frac{g_0}{1 + g_0 I_{\text{lat}}}. \quad (C6)$$

Comparing equations (C3) and (C6), one can see that \tilde{g}_0 plays the role of the effective bare coupling g_c if the original lattice problem is mapped to the continuum Lieb-Liniger model. The value of \tilde{g}_0 will, e.g., determine the phase shifts in two-body scattering. As long as the coupling constant g_0 is small, such a mapping presents no problem. However, it is easy to see that if I_{lat} is negative and $g_0|I_{\text{lat}}|$ becomes close or exceeds 1, then even the sign of \tilde{g}_0 can differ from that of the lattice bare coupling g_0 . The parameter \tilde{g}_0 can be directly interpreted as the effective continuum bare coupling only if the condition

$$|\tilde{g}_0|m \ll 1 \quad (C7)$$

is satisfied, otherwise one has to look at the dressed coupling $\Gamma(\Lambda_*)$.

Appendix D: Schrödinger's equation for the two-magnon scattering problem

We set the magnetic field at the saturation value,²⁹ $H = H_S = 2S(J_1^z + J_2^z) + S(J_1^2 + 8J_2^2)/4J_2$ and consider a general two-magnon state that can be written in the following form (here we use a normalization different from that of Ref. 22):

$$|\Psi_{2M}\rangle = \sum_{n, m \geq n} c_{n, m} \frac{S_n^- S_m^- |F\rangle}{\langle F | S_m^\dagger S_n^\dagger S_n^- S_m^- | F \rangle}, \quad (D1)$$

where $|F\rangle$ is the fully polarized state. The total quasi-momentum K is conserved, therefore one can separate the center of mass motion by setting $c_{n, m} = \exp(i \frac{n+m}{2} K) C_{m-n}$. Solving the Schrödinger equation $\mathcal{H}|\Psi_{2M}\rangle = E|\Psi_{2M}\rangle$ for scattering states in the thermodynamic limit, one can identify the energy $E = \varepsilon(k_1) + \varepsilon(k_2) + E_F$, where $E_F = N(S^2(J_1^z + J_2^z) - H_S S)$ is the energy of the fully polarized state, as

$$E = \Omega_0 - 2SJ(Q) + E_F, \\ \Omega_0/4S = J_1 \cos(k) \cos \frac{K}{2} + J_2 \cos(2k) \cos(K), \quad (D2)$$

where k_1, k_2 are the magnon momenta, $k = \frac{1}{2}(k_1 - k_2)$ is one half of the relative momentum, and $K = k_1 + k_2$ is the total momentum. The Schrödinger equation leads to the following linear system for the amplitudes C_r :

$$\begin{aligned}
\Omega_0 C_0 &= 2\sqrt{S(2S-1)}(J_1 C_1 \cos \frac{K}{2} + J_2 C_2 \cos K), \\
(\Omega_0 - J_1^z) C_1 &= 2J_1 \sqrt{S(2S-1)} C_0 \cos \frac{K}{2} + 2SJ_1 C_2 \cos \frac{K}{2} + 2SJ_2(C_1 + C_3) \cos K, \\
(\Omega_0 - J_2^z) C_2 &= 2J_2 \sqrt{S(2S-1)} C_0 \cos K + 2SJ_2 C_4 \cos K + 2SJ_1(C_1 + C_3) \cos \frac{K}{2}, \\
\Omega_0 C_r &= 2SJ_1 \cos \frac{K}{2} (C_{r+1} + C_{r-1}) + 2SJ_2 \cos K (C_{r+2} + C_{r-2}) \quad (r \geq 3).
\end{aligned} \tag{D3}$$

Appendix E: Scattering phase shift in the interspecies scattering problem

To extract the phase shift for the interspecies scattering problem from the solution (28), we put $k = Q + p$ and consider the limit of small deviation from the minimum of dispersion $p \rightarrow 0$, then $\tilde{k} = Q - p + O(p^2)$ and the scattering state Eq.(28) can be rewritten as follows,

$$\begin{aligned}
C_r = & \sqrt{\cos^2 \alpha + (v + \sin \alpha)^2} \cos(Qr) \cos(pr + \delta_{12}) \\
& - \sqrt{\cos^2 \alpha + (v - \sin \alpha)^2} \sin(Qr) \sin(pr - \gamma) \quad (\text{E1})
\end{aligned}$$

where

$$\begin{aligned}
\delta_{12} &= -\arccos \frac{\cos \alpha}{\sqrt{\cos^2 \alpha + (v + \sin \alpha)^2}}, \\
\gamma &= -\arccos \frac{\cos \alpha}{\sqrt{\cos^2 \alpha + (v - \sin \alpha)^2}}. \quad (\text{E2})
\end{aligned}$$

From the form (E1) one can easily guess that for $J_1 = 0$ ($Q = \pi/2$) the scattering phase shift is δ_{12} . This is indeed so, because to obtain the phase shift we have to put $r = 2n$ and the second term in Eq. (E1) vanishes (for odd values $r = 2n + 1$ there is no scattering involved

since at $J_1 = 0$ the system corresponds to two decoupled chains).

For $Q = 0$ (i.e., at the ferromagnetic Lifshitz point $\beta = -4$) and $Q = \pi$ (the antiferromagnetic Lifshitz point $\beta = 4$) it is also easy to recognize δ_{12} as the scattering phase shift.

Furthermore, for general values of β one can show that $\lim_{p \rightarrow 0} \alpha = \pm \pi/2$ and $\lim_{p \rightarrow 0} v = \pm 1$, so that $\lim_{p \rightarrow 0} (v - \sin \alpha) = \lim_{p \rightarrow 0} \cos \alpha = 0$. This corresponds to the fact that scattering states vanish when $p \rightarrow 0$, i.e., when the magnon momenta tend to the dispersion minima $k_1 \rightarrow Q$, $k_2 \rightarrow -Q$, and reflects the fermionization of excitations forming a single Fermi sea, as mentioned in the main text. It is easy to see that the second amplitude in Eq. (E1) tends to zero, $\lim_{p \rightarrow 0} \sqrt{\cos^2 \alpha + (v - \sin \alpha)^2} = 0$, while the first amplitude tends to a constant, $\lim_{p \rightarrow 0} \sqrt{\cos^2 \alpha + (v + \sin \alpha)^2} = 2$. Thus, the scattering phase shift for interspecies scattering at $p \rightarrow 0$ is given by δ_{12} for any β .

One can also show that the two following expressions are equal to each other,

$$\lim_{p \rightarrow 0} \frac{\cot(\delta_{12})}{p} = \lim_{p \rightarrow 0} \frac{\cot(\alpha)}{2p}. \tag{E3}$$

In other words, if $\alpha \rightarrow -\pi/2 + 2a_{12}p$ at $p \rightarrow 0$, then $\delta_{12} \rightarrow -\pi/2 + a_{12}p$.

-
- ¹ *Frustrated Spin Systems*, ed. by H.T. Diep (World Scientific, 2004).
 - ² *Introduction to Frustrated Magnetism: Materials, Experiments, Theory*, ed. by C. Lacroix, P. Mendels, and F. Mila (Springer Series in Solid-State Sciences **164**, 2011).
 - ³ A. V. Chubukov, Phys. Rev. B **44**, 4693 (1991).
 - ⁴ F. Heidrich-Meisner, A. Honecker, and T. Vekua, Phys. Rev. B **74**, 020403(R) (2006).
 - ⁵ T. Vekua, A. Honecker, H.-J. Mikeska, and F. Heidrich-Meisner, Phys. Rev. B **76**, 174420 (2007).
 - ⁶ T. Hikihara, L. Kecke, T. Momoi, and A. Furusaki, Phys. Rev. B **78**, 144404 (2008).
 - ⁷ J. Sudan, A. Lüscher, and A. M. Läuchli, Phys. Rev. B **80**, 140402(R) (2009).
 - ⁸ K. Okunishi and T. Tonegawa, J. Phys. Soc. Japan **72**, 479 (2003).
 - ⁹ A. Kolezhuk and T. Vekua, Phys. Rev. B **72**, 094424 (2005).
 - ¹⁰ I. P. McCulloch, R. Kube, M. Kurz, A. Kleine, U.

-
- Schollwöck, and A. K. Kolezhuk, Phys. Rev. B **77**, 094404 (2008).
 - ¹¹ K. Okunishi, J. Phys. Soc. Japan **77**, 114004 (2008).
 - ¹² T. Hikihara, T. Momoi, A. Furusaki, and H. Kawamura, Phys. Rev. B **81**, 224433 (2010).
 - ¹³ K. Okunishi, Y. Hieida, and Y. Akutsu, Phys. Rev. B **60**, R6953 (1999).
 - ¹⁴ F. Heidrich-Meisner, I. P. McCulloch, and A. K. Kolezhuk, Phys. Rev. B **80**, 144417 (2009); *ibid.* **81**, 179902 (2010).
 - ¹⁵ M. Enderle, C. Mukherjee, B. Fåk, R. K. Kremer, J.-M. Broto, H. Rosner, S.-L. Drechsler, J. Richter, J. Malek, A. Prokofiev, W. Aßmus, S. Pujol, J.-L. Raggazzoni, H. Rakoto, M. Rheinstädter, and H. M. Rønnow, EPL **70**, 237 (2005).
 - ¹⁶ N. Büttgen, H.-A. Krug von Nidda, L. E. Svistov, L. A. Prozorova, A. Prokofiev, and W. Aßmus, Phys. Rev. B **76**, 014440 (2007).
 - ¹⁷ L. E. Svistov, T. Fujita, H. Yamaguchi, S. Kimura, K. Omura, A. Prokofiev, A. I. Smirnov, Z. Honda and M.

- Hagiwara, JETP Lett. **93**, 21 (2010).
- ¹⁸ M. E. Zhitomirsky and H. Tsunetsugu, Europhys. Lett. **92**, 37001 (2010).
 - ¹⁹ M. Hase, H. Kuroe, K. Ozawa, O. Suzuki, H. Kitazawa, G. Kido, and T. Sekine, Phys. Rev. B **70**, 104426 (2004).
 - ²⁰ S.-L. Drechsler, O. Volkova, A. N. Vasiliev, N. Tristan, J. Richter, M. Schmitt, H. Rosner, J. Málek, R. Klingeler, A. A. Zvyagin, and B. Büchner, Phys. Rev. Lett. **98**, 077202 (2007).
 - ²¹ M. G. Banks, R. K. Kremer, C. Hoch, A. Simon, B. Oulad-diaf, J.-M. Broto, H. Rakoto, C. Lee, and M.-H. Whangbo, Phys. Rev. B **80**, 024404 (2009).
 - ²² M. Arlego, F. Heidrich-Meisner, A. Honecker, G. Rossini, and T. Vekua, Phys. Rev. B **84**, 224409 (2011).
 - ²³ F. Heidrich-Meisner, I. A. Sergienko, A. E. Feiguin, and E. R. Dagotto, Phys. Rev. B **75**, 064413 (2007).
 - ²⁴ A. K. Kolezhuk and I. P. McCulloch, Condensed Matter Physics **12**, 429 (2009).
 - ²⁵ G. Fáth and P. B. Littlewood, Phys. Rev. B **58**, R14709 (1998).
 - ²⁶ S. R. White, Phys. Rev. Lett. **69**, 2863 (1992); Phys. Rev. B **48**, 10345 (1993).
 - ²⁷ U. Schollwöck, Rev. Mod. Phys. **77**, 259 (2005).
 - ²⁸ The use of Dyson-Maleev representation which leads to a non-hermitean bosonic Hamiltonian is not important but merely convenient. The exact ladder structure of the Bethe-Salpeter equation means that we are in fact solving a two-body problem (repeated scattering of two particles). One could thus use the Goldhirsch representation⁵⁷ for spin operators and neglect terms of higher than quartic order in the bosonic Hamiltonian, which leads to a hermitean Hamiltonian for general spin S , but with slightly more cumbersome coefficients. We have explicitly checked that the final results do not depend on the chosen representation.
 - ²⁹ If magnons form bound states, the actual saturation field (minimal strength of magnetic field needed to fully polarize the ground state) differs from H_s by the magnon binding energy.
 - ³⁰ D. Uzunov, Phys. Lett. **A87**, 11 (1981).
 - ³¹ E. G. Batyev and L. S. Braginskii, Zh. Eksp. Teor. Fiz. **87**, 1361 (1984) [Sov. Phys. JETP **60**(4), 781 (1984)].
 - ³² H. T. Ueda and K. Totsuka, Phys. Rev. B **80**, 014417 (2009).
 - ³³ S. Gluzman, Phys. Rev. B **50**, 6264 (1994).
 - ³⁴ T. Nikuni and H. Shiba, J. Phys. Soc. Japan **64**, 3471 (1995).
 - ³⁵ G. Jackeli and M. E. Zhitomirsky, Phys. Rev. Lett. **93**, 017201 (2004).
 - ³⁶ K. Okunishi, Y. Hieida, and Y. Akutsu, Phys. Rev. B **59**, 6806 (1999).
 - ³⁷ M. D. Johnson and M. Fowler, Phys. Rev. B **34**, 1728 (1986).
 - ³⁸ D. S. Fisher and P. C. Hohenberg, Phys. Rev. B **37**, 4936 (1988).
 - ³⁹ D. R. Nelson and H. S. Seung, Phys. Rev. B **39**, 9153 (1989).
 - ⁴⁰ E. B. Kolomeisky and J. P. Straley, Phys. Rev. B **46**, 11749 (1992).
 - ⁴¹ E. B. Kolomeisky, T. J. Newman, J. P. Straley, and X. Qi, Phys. Rev. Lett. **85**, 1146 (2000).
 - ⁴² A. K. Kolezhuk, Phys. Rev. A **81**, 013601 (2010).
 - ⁴³ In Ref. 9, there is a mistake in Eq. (21), leading to the erroneous impression that in the isotropic chain g_{12} may become smaller than g_{11} in the semiclassical limit $S \rightarrow \infty$.
 - ⁴⁴ M. Girardeau, J. Math. Phys. **1**, 516 (1960).
 - ⁴⁵ M. D. Lee, S. A. Morgan, M. J. Davis, and K. Burnett, Phys. Rev. A **65**, 043617 (2002); see also arXiv:cond-mat/0305416 (unpublished).
 - ⁴⁶ S. A. Morgan, M. D. Lee, and K. Burnett, Phys. Rev. A **65**, 022706 (2002).
 - ⁴⁷ M. Olshanii, Phys. Rev. Lett. **81**, 938 (1998).
 - ⁴⁸ The property of reformionization with a common Fermi sea in the TLL2 phase applies only in the limit of vanishing density, when it is not possible to use the Luttinger liquid description (in the dilute limit the fixed point of the renormalization group flow is a theory of non-relativistic free fermions with the dynamical critical exponent $z = 2$). This has to be contrasted with the situation at finite density, when the hydrodynamic regime develops and the TLL2 state is governed by the fixed point of two decoupled Gaussian models (two copies of Tomonaga-Luttinger liquids).
 - ⁴⁹ F. H. L. Essler, H. Frahm, F. Göhmann, A. Klümper, and V. E. Korepin, *The One-Dimensional Hubbard Model* (Cambridge University Press, 2005).
 - ⁵⁰ A. Seel, T. Bhattacharyya, F. Göhmann, and A. Klümper, J. Stat. Mech. P08030 (2007).
 - ⁵¹ G.E. Astrakharchik, D. Blume, S. Giorgini, and B.E. Granger, Phys. Rev. Lett. **92**, 030402 (2004); M.T. Batchelor, M. Bortz, X.W. Guan, and N. Oelkers, J. Stat. Mech. L10001 (2005); G.E. Astrakharchik, J. Boronat, J. Casulleras, and S. Giorgini, Phys. Rev. Lett. **95**, 190407 (2005).
 - ⁵² Actually, the lowest energy of a two-magnon bound state in the isotropic ferromagnetic $S = \frac{1}{2}$ frustrated chain is reached at $K = \pi - \delta(\beta)$ with $\delta \ll 1$, for $-4 < \beta < -2.67$, and for $-2.67 < \beta < 0$ the minimum of the bound state dispersion lies at $K = \pi$.⁵⁸ For that reason, our theory is not directly applicable to this case.
 - ⁵³ G. Vidal, J. I. Latorre, E. Rico, and A. Kitaev, Phys. Rev. Lett. **90**, 227902 (2003).
 - ⁵⁴ P. Calabrese and J. Cardy, J. Stat. Mech. P06002 (2004).
 - ⁵⁵ S. Nishimoto, Phys. Rev. B **84**, 195108 (2011).
 - ⁵⁶ J. Zinn-Justin, *Quantum Field Theory and Critical Phenomena* (Oxford Univ. Press, 2002), §A7.2 (p.180).
 - ⁵⁷ I. Goldhirsch, E. Levich, and V. Yakhot, Phys. Rev. B **19**, 4780 (1979); I. Goldhirsch, J. Phys. A **13**, 453 (1980).
 - ⁵⁸ R. O. Kuzian and S.-L. Drechsler, Phys. Rev. B **75**, 024401 (2007).